DESIGN STRATEGIES FOR LOW THRUST TRANSFERS IN THE EARTH-MOON SYSTEM

by

Liam Fahey

A Thesis

Submitted to the Faculty of Purdue University

In Partial Fulfillment of the Requirements for the degree of

Master of Science in Aeronautics and Astronautics

School of Aeronautics and Astronautics

West Lafayette, Indiana

December 2024

THE PURDUE UNIVERSITY GRADUATE SCHOOL
STATEMENT OF COMMITTEE APPROVAL

Dr. Kathleen C. Howell, Chair

School of Aeronautics and Astronautics

Dr. Carolin Frueh

School of Aeronautics and Astronautics

Dr. Kenshiro Oguri

School of Aeronautics and Astronautics

Approved by:

Dr. Dengfeng Sun

ACKNOWLEDGMENTS

First I would like to thank my loved ones. Thank you to my parents for all your support during this process. You taught me from a young age the joys of learning, the value of kindness, and the strength of asking for help. These lessons have made my graduate studies and life in general much easier. Thank you for supporting my last minute decision to study here at Purdue, it was an easy decision when I knew you supported it. Additionally, thank you to my girlfriend, Nicole. You have brought so much joy to my life and I'm excited to continue my education knowing you are with me. Lastly, thank you to Aunt Linda, Uncle Jeremy, Grace, and Luca. You made West Lafayette feel like home.

Thank you to my advisor, Professor Kathleen Howell. You have provided incredible insights throughout the research process. I could not have done it without you. I am honored to be a part of your research group and I look forward to continuing to learn from you and my colleagues.The research presented in this thesis would not have been possible without the insights, questions, and suggestions of my friends in the Multi Body Dynamics Research Group. I am so thankful for your perspective and technical knowledge which guided much of this investigation. I would also like to thank my committee members, Professor Carolin Frueh and Kenshiro Oguri for their contributions. Your perspective has greatly improved the quality of this thesis.

Lastly, I would like to thank Purdue University Residents for funding my education and The Center for Academic Vision and Enrichment for providing an additional work opportunity for me. The flexibility of these jobs allowed me to focus on my academics and the opportunities to work with students just beginning their academic careers helped preserve my passion for learning.

TABLE OF CONTENTS

LIST OF TABLES

LIST OF FIGURES

ABSTRACT

The increased interest in deep space missions is creating an increased interest in cislunar space. The need for fast and efficient methods of traversing the lunar vicinity increases as more spacecraft enter the region. This investigation discusses methods of low thrust transfer design in order to create low cost and low time of flight transfers. Indirect optimization is employed to compute minimum energy and minimum fuel transfers in the circular restricted three body problem. Sigmoid smoothing techniques are leveraged to approximate the optimal bang-coast-bang solution with continuous functions. The minimum fuel solution is employed as an initial guess to target an inertially fixed thrust direction transfer. This process is applied to a variety of cislunar orbital transfer problems. Transfers are constructed between orbits in the L_1 halo, L_2 halo, distant retrograde, and L_4 short period orbit families. The resulting trajectories are compared to impulsive and free transfers from the literature based on the required propellant mass and time of flight.

1. INTRODUCTION

1.1 Problem Definition

In recent years, more missions involve spacecraft moving to explore deep space and, consequently facing greater technical challenges. These challenges tend to fall into three categories, dynamical, numerical, and hardware. Dynamically the deep space environment is relatively unstable and often chaotic compared to spacecraft behavior near Earth. This behavior cannot be accurately modeled by mathematical expressions with analytical solutions. Numerical technics must be leveraged in order to understand spacecraft motion that often come with challenges in accuracy. Lastly, low-thrust engines are often desireable on spacecraft undergoing missions that require higher propellant efficiency. The low thrust hardware results in better efficiency at a cost to maximum thrust acceleration. These challenges often present difficulties for common mission design techniques, that generally leverage the relatively stable dynamics of the near Earth gravity field and nearly impulsive engines.

An increasing number of space missions are exploring regions where the gravitational forces acting on the spacecraft are not dominated by a single celestial body. Rather, multiple celestial bodies can introduce forces on the spacecraft with similar magnitudes. In the Artemis missions, for example, the spacecraft leverage the gravity of both the Earth and the Moon [1]; then, the Capstone vehicle, acting as a pathfinder is currently in the 9:2 Near Rectilinear Halo Orbit (NRHO) [2] to be later occupied by Gateway during Artemis IV and beyond [1], [3]. These mission scenarios incorporate orbits that only exist within a model including both the Earth and the Moon gravity, and possibly the Sun. Additionally, the James Webb space telescope is current in a Sun-Earth Halo orbit where the Sun and Earth gravity are both integral in defining the telescopes motion [4]. Various other missions are designed specifically for cislunar space including IM-1 [5], Chandrayaan-3 [6], and SLIM [7]. These missions necessitate an understanding of the dynamics impact of multiple bodies simultaneously to ensure their success. While the dynamics are more complex more spacecraft are leveraging the added efficiency of low-thrust engines to reduce the propellant cost. The Dawn [8], Deep Space 1 [9], and lunar IceCube missions [10] all involved low-thrust spacecraft. Additionally, the plan for the NASA Gateway space station, is to leverage low-thrust

to transfer from Earth to the 9:2 NRHO [3]. Such engines are not modeled with instantaneous changes in velocity, but require a significant time when thrust is active to control their trajectory through space.

Overall, these changes generally increase spacecraft efficiency by notably reducing propellant requirements, however probable propellant savings comes at a cost to the trajectory design process resulting in a conventional analysis approach that is inaccurate. This investigation offers various techniques for introducing low-thrust modeling in more complex dynamical environments to achieve lower-cost transfers between orbits within the context of a multi-body model, specifically in the Earth-Moon-spacecraft three-body problem.

1.2 Previous Work

1.2.1 Multi-body Dynamics

A number of dynamical models are employed to understand the behavior of a spacecraft in a multi-body environment. The problem was formally analyzed by Newton in Philosophiae Naturalis Principia Mathematica [11]. The analysis presented in this document employs a model comprised of three mutually influenced gravitational bodies, formally labelled the restricted 3 body problem (R3BP). This model was first formulated by Euler [12]. Many notable mathematicians focused on understanding the dynamical behavior within the context of the model. Lagrange identified additional equilibrium points that are now named for him [12]. Jacobi determined the existence of an integral of motion in th restricted problem [13], and Hill modeled the motion of the Moon as it is acted upon by the gravity of the Earth and Sun, as well as defined regions of exclusion based on the Jacobi integration constant [14]. Poincare developed the foundation for dynamic systems theory, proved that the Jacobi Constant is the only integral of motion in th restricted problem and that the n-body problem does not have a closed form solution [15].

The Circular Restricted 3-Body Problem (CR3BP) is selected as a reasonable model for this investigation due to its simplicity, while still capturing the motion of satellites in cislunar space. However, other models exist, for example the elliptic restricted 3 body problem (ER3BP) and Hills restricted model (HR3BP), which also describe 3 body dynamics. The

ER3BP assumes elliptic motion of the Moon and Earth rather than circular, while the HR3BP defines the motion of the moon based on the description by Hill. These models include more accurate descriptions of the Earth-Moon motion, however the added complexity is unnecessary for the problems addressed in this document.

The behaviors within the CR3BP are well studied. The advancements in computational power of the 20th century allowed for the computation of several families of periodic orbits. Orbit families are computed in the CR3BP by Breakwell and Brown [16] using numerical methods. Additional analysis of periodic orbits as well as new families are discussed by Howell [10] and Henon [17]. After a variety of families were computed researchers began searching for transfers between them. Koon [18] and Parker [19] computed free transfers between planar orbit families. Their methods leveraged the natural instability periodic orbits to produce free transfers. These types of transfers are also computed for spatial orbits by Haapala [20]. Additionally, she, as well as others have computed impulsive transfers between many orbits in multiple orbit families.

1.2.2 Low-Thrust Transfer Design

The inclusion of low-thrust in the transfer design process leads to infinitely many solutions. While having multiple options is useful, many of thee solutions have overly large propellant requirements. The large solution space must be reduced to an optimal solution. Lawden applies the calculus of variation to reformulate the optimal transfer design process as a 2 point boundary value problem [21]. Descriptions for generating these types of transfers can be found in Spacecraft Trajectory Optimization [22]. These techniques are formulated in the 2-body problem however they have been applied to orbits in the CR3BP by Stuart and Ozimek [23], Senent [24], and more recently, Parrish [25].

This document leverages indirect optimization to find the optimal solution through an implementation of the calculus of variation. Unlike direct optimization, indirect optimization does not compute the function itself but rather produces criteria for the function's derivative. This form of optimization is discussed in depth by Longuski in Optimal Control with Aerospace applications [26]. The greatest challenge in indirect optimization is in selecting

an initial guess for the 2 point boundary value problem (2PBVP) created by the method. However, Parish and others has examined forming initial guesses with adjoint control, machine learning, and natural flow dynamics [25]. Additionally, Cox [27] and Pino [28] analyzed energy informed approaches within the ballistic dynamics to form initial guesses.

1.3 Overview

The goal of this work is to describe a methodology for constructing extremely low cost low-thrust transfers between libration point orbits in the CR3BP. The natural structures in the CR3BP are used as initial guesses that are then converted to optimal transfers using indirect optimization. The document is organized as follows:

- **Chapter 2:** The CR3BP is described including it's underlying assumptions and coordinate frames. The affects of an additional low thrust term on the equations of motion is also discussed. As well as, the symmetry of the models and constant of integration.
- **Chapter 3:** General techniques for understanding the natural structures within dynamic systems are presented and applied to the CR3BP and low thrust model. This includes periodic orbits, invariant manifolds and stretching directions.
- **Chapter 4:** Indirect Optimization problem strategies are considered such as Euler-Lagrange Theorem and the construction of the hamiltonian. The Transversality condition is discussed for its role in computing optimal initial and final criteria when necessary.
- **Chapter 5:** The minimum energy and minimum fuel transfer problems are derived for transfers between orbits. A homotopy in the sigmoid function is employed to continue solutions toward the minimum fuel problem and finally the solutions are altered to thrust in an inertially fixed direction to meet operational constraints.
- **Chapter 6:** Transfers produced through the methods in chapter 5 are discussed. This includes transfers between members of the same family leveraging intermediate orbits as initial guesses as well as transfers between different families using their stable and

unstable manifolds, or stretching directions if stable and unstable manifolds are not present.

- **Chapter 7:** This chapter makes concluding remarks on the transfer methodology included challenges and strengths, followed by a layout for potential future work in optimal low-thrust transfers in multi-body dynamical models.

2. DYNAMIC MODELS

The mathematical models that describe spacecraft motion for transfer applications are formulated in this chapter. First, The Circular Restricted 3 Body Problem (CR3BP) is derived to describe the motion of a spacecraft influenced by the gravitational forces of the Earth and Moon assuming they move on circular orbits relative to each other. A rotating frame is constructed in such a way that the Earth and Moon are fixed when viewed in the new frame. This view and the mathematical model renders an autonomous system. The symmetry of the equations of motion in this formulation is discussed and the locations of the five equilibrium points are derived. Lastly, the integral of motion is identified. A second model of interest is the CR3BP with additional low thrust terms. The CR3BP with Low Thrust (CR3BP+LT) is constructed for use in low thrust transfer design. The impact of low thrust on the CR3BP integral of motion is derived for an arbitrary thrust direction and an inertially fixed thrust model is formulated based on the rotation matrix between the inertial and rotating frames.

2.1 Circular Restricted three-Body Problem

The circular restricted three body-model is employed to describe the dynamic motion that arises from the gravitational fields of two bodies acting on a third smaller body. Frequently, the CR3BP is employed to model behavior in cislunar space. In this regime, neither the Earth nor the Moon gravity is of sufficiently small magnitude to neglect. The CR3BP is formulated with a few key assumptions that simplify the dynamics. The simplified model allows for the existence of equilibrium points, symmetry, and an integral of motion that are leveraged in the transfer design process.

The first assumption in constructing the CR3BP equations of motion is that the only forces modeled are the mutual gravitational attraction between the bodies. Next the third body is assumed to be much smaller than the other two. The two larger bodies are denoted the primaries. The result of this assumption is that the primary motion is not affected by the third body gravity. Therefore, the primaries behavior is modeled as keplarian with analytical solutions in the form of conic sections. The third assumption is that the motion of the primaries is circular about their common barycenter. Although not required, circular

primary orbits allow an integral of the motion. The CR3BP is frequently applied in cislunar space to model spacecraft behavior. For these applications, the Earth and Moon are the two primaries and the spacecraft is the third body.

The derivation of the mathematical model governing the CR3BP begins with the forces on each body. Newton's Second Law delivers the differential equations as

$$m_1 \bar{R}_1'' = -G\left(\frac{m_1 m_2}{|\bar{R}_{21}|^3}\bar{R}_{21} + \frac{m_1 m_3}{|\bar{R}_{31}|^3}\bar{R}_{31}\right) \tag{2.1}$$

$$m_2 \bar{R}_2'' = -G\left(\frac{m_1 m_2}{|\bar{R}_{21}|^3}\bar{R}_{21} + \frac{m_2 m_3}{|\bar{R}_{32}|^3}\bar{R}_{32}\right) \tag{2.2}$$

$$m_3 \bar{R}_3'' = -G\left(\frac{m_1 m_3}{|\bar{R}_{31}|^3}\bar{R}_{31} + \frac{m_2 m_3}{|\bar{R}_{32}|^3}\bar{R}_{32}\right) \tag{2.3}$$

In these equations the primaries are denoted with subscripts '1' and '2', such that '1' refers to the larger primary. The mass of each body is denoted 'm'. The position vector of each body, expressed as 'R' has the first subscript indicating the target body and the second indicating the observer. When only one subscript is present the position vector is relative to an arbitrary initially fixed point. A diagram of a representation of the three-body problem appears in Figure 2.1 in an arbitrary inertial frame.

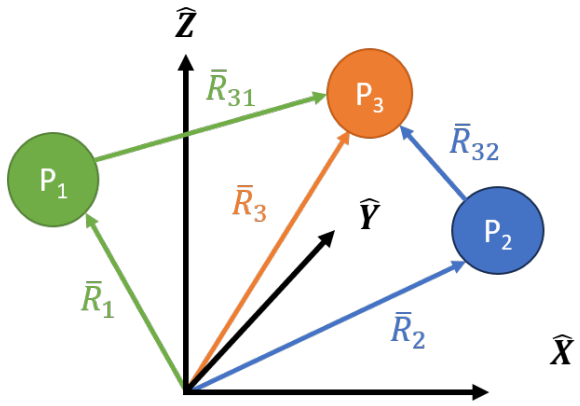

Figure 2.1. The force felt on an object in the gravitational fields of 2 primary bodies in an arbitrary inertial frame

In the CR3BP, the motion of the primaries is assumed circular. As a result, Equations (2.1) and (2.2), are unnecessary as they describe motion that is already determined by this assumption. Equation (2.3) is the key differential equation to determine the motion of the third body. The equation is divided through by m_3 to produce

$$\bar{R}_3'' = -G\left(\frac{m_1}{|\bar{R}_{31}|^3}\bar{R}_{31} + \frac{m_2}{|\bar{R}_{32}|^3}\bar{R}_{32}\right) \tag{2.4}$$

Equation (2.4) is the acceleration of the third body as observed in the arbitrary inertial frame. This differential equation does not possess an analytic solution, thus numerical integration is required to produce solutions.

Nondimensionalizing the equations of motion via characteristic quantities ensures all state elements remain within a similar magnitude range thereby improving the accuracy of the numerical integration process. The characteristic quantities include l^*, the length between the primaries, m^*, the sum of the mass of the primaries, and t^*, the characteristic time. The characteristic time is selected such that the non-dimensional gravitational constant G is equal to one. The equations for these quantities are

$$m^* = m_1 + m_2 \tag{2.5}$$

$$l^* = |\bar{R}_{21}| \tag{2.6}$$

$$t^* = \sqrt{\frac{l^{*3}}{Gm^*}} \tag{2.7}$$

For convenience the mass ratio is defined as

$$\mu = \frac{m_2}{m^*} \tag{2.8}$$

These characteristic quantities are employed to express the equations of motion in nondimensional units. The nondimensional positions of the third body relative to the system barycenter, larger primary, and smaller primary are then $\bar{r}_3$, $\bar{r}_{31}$, and $\bar{r}_{32}$, respectively. The magnitudes of $\bar{r}_{31}$ and $\bar{r}_{32}$ are labelled d and r. The time derivatives are with respect to nondimensional time, i.e. t, rather than dimensional time. To differentiate the different time

derivatives, the apostrophe nomenclature denotes dimensional time derivatives, while the nondimensional time derivative is written as $\frac{d}{dt}$. The nondimensional equation of motion for the third body as observed from inertial space is

$$\frac{d^2\bar{r}_3}{dt^2} = -\left(\frac{(1-\mu)}{d^3}\bar{r}_{31} + \frac{\mu}{r^3}\bar{r}_{32}\right) \tag{2.9}$$

The location of the third body relative to the primaries is time dependant in the inertially fixed frame therefore Equation (2.9) represents a non-autonomous system.

The formulation shifts the view to a rotating frame, based on the motion of the primaries to enable an autonomous system of equations. The $\hat{x}$ direction is defined as the vector from the larger to the smaller primary. The direction of the primaries angular momentum about their barycenter is parallel to $\hat{z}$ and $\hat{y}$ completes the right-hand triad. In this view, the primaries remain on the x axis and the circular primary orbit assumption ensures that the primaries are fixed in the frame. The rotating frame appears in Figure 2.2.

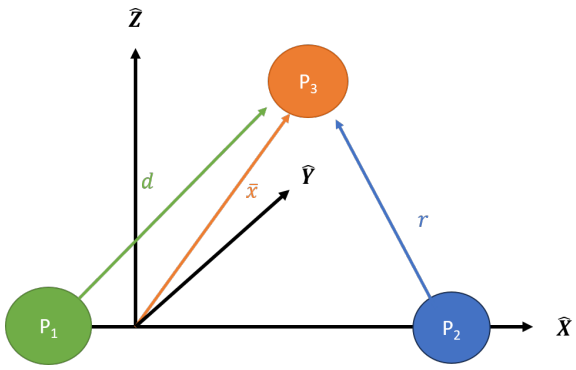

Figure 2.2. Gravitational forces felt by a body in the CR3BP viewed in a rotating frame

Transport theorem is employed to express the acceleration of the third body as initially defined with respect to the inertial frame in terms of the rotating frame. This relation is

$$\frac{d\bar{r}^I}{dt} = \frac{d\bar{r}^R}{dt} + \bar{n} \times \bar{r} \tag{2.10}$$

Superscripts refer to the frame of differentiation and $\bar{n}$ is the relative rotation vector between the frames. Based on transport theorem, the inertial acceleration is expressed in terms of the rotating quantities as

$$\frac{d^2\bar{r}_3}{dt^2} = \begin{bmatrix} \ddot{x} - 2\dot{y}n - xn^2 \\ \ddot{y} + 2\dot{x}n - yn^2 \\ \ddot{z} \end{bmatrix} \tag{2.11}$$

State elements in the rotating frame are refereed to as $[x, y, z]$ and dot notation is employed for nondimensional time derivatives in the rotating frame. Due to the definition of nondimensional time the frame rotation rate n is 1. Therefore the equations of motion can be written as

$$\ddot{x} = 2\dot{y} + x - \frac{(1-\mu)(\mu+x)}{d^3} - \frac{\mu(x-1+\mu)}{r^3} \tag{2.12}$$

$$\ddot{y} = -2\dot{x} + y - \frac{(1-\mu)(y)}{d^3} - \frac{\mu y}{r^3} \tag{2.13}$$

$$\ddot{z} = -\frac{(1-\mu)(z)}{d^3} - \frac{\mu z}{r^3} \tag{2.14}$$

Equations (2.12) to (2.14) are the governing equations for the behavior of a third body acted upon by the the gravity of two primary bodies as viewed in a rotating frame.

Often it is advantageous to analyze a subset of the system rather than the entire 6 dimensional system. For the CR3BP the z equation can be removed to create a 4 dimensional subsystem. The only state elements that occur in the numerator of Equation (2.14) are z and $\dot{z}$. Therefore setting z and $\dot{z}$ to zero ensure that the elements remain zero for all time. Any state with zero z and $\dot{z}$ elements remains on the x-y plane within a subsystem denoted the planar CR3BP. The CR3BP equations of motion also posses useful symmetries that are exploited during the mission design process. The mirror theorem by Roy and Ovenden [29] guarantees that the system has forward-backward time symmetry as stated,

Theorem 2.1.1. *If n point-masses are acted upon by their mutual gravitational forces only, and at a certain epoch each radius vector from the (assumed stationary) centre of mass of*

the system is perpendicular to every velocity vector, then the orbit of each mass after that epoch is a mirror image of its orbit prior to that epoch.

In the CR3BP, configurations that meet the criteria of Theorem 2.1.1 occur when the third body is on the x-z plane with velocity purely in the y direction or on the x-axis with zero velocity in the x direction.

An import feature of any dynamic system is the existence and location of equilibrium points. The CR3BP has five equilibrium points. The first three located on the x-axis are known as the co-linear lagrange points that result from setting y and z to zero and solving the resulting 1-D root problem given in

$$x = \frac{(1-\mu)(x+\mu)}{|x+\mu|^3} + \frac{\mu(x-1+\mu)}{|x-1+\mu|^3} \tag{2.15}$$

The signs of the absolute value terms in Equation (2.15) have ambiguity that depends on the location relative to the primaries. A different lagrange point is computed depending on the signs of these terms. The equations for L_1, between the primaries, L_2, to the right of P_2, and L_3, to the left of P_1 are given as

$$x = \frac{1-\mu}{(x+\mu)^2} - \frac{\mu}{(x-1+\mu)^2} \tag{2.16}$$

$$x = \frac{1-\mu}{(x+\mu)^2} + \frac{\mu}{(x-1+\mu)^2} \tag{2.17}$$

$$x = -\frac{1-\mu}{(x+\mu)^2} - \frac{\mu}{(x-1+\mu)^2} \tag{2.18}$$

respectively. The additional two equilibrium points are found by assuming y is not zero. Therefore Equation (2.13) can be divided through by y resulting in

$$1 = \frac{1-\mu}{d^3} + \frac{\mu}{r^3} \tag{2.19}$$

Next Equation (2.12) is expanded and rearranged to form

$$x = \frac{x(1-\mu)}{d^3} + \frac{x\mu}{r^3} + \frac{\mu(1-\mu)}{d^3} + \frac{\mu\mu}{r^3} - \frac{\mu}{r^3} \tag{2.20}$$

and

$$0 = x\left[\frac{1-\mu}{d^3} + \frac{\mu}{r^3} - 1\right] + \mu[\frac{1-\mu}{d^3} + \frac{\mu}{r^3}] - \frac{\mu}{r^3} \tag{2.21}$$

Notice that according to Equation (2.19) the term in the first bracket of Equation (2.21) is 0 and the term in the second bracket is 1 resulting in

$$0 = \mu - \frac{\mu}{r^3} \tag{2.22}$$

Equation (2.22) can only be true if $r = 1$. this value for r is then plugged back into Equation (2.19) producing

$$0 = 1 - \frac{1-\mu}{d^3} + \mu \tag{2.23}$$

Equation (2.23) can only be true if $d = 1$. Therefore, additional equilibrium points exist at a nondimensional distance of 1 from both of the primaries. The only two locations at these distances form equilateral triangles with the primaries. Figure 2.3 is a diagram of the lagrange points locations in the CR3BP and Table 2.1 gives their locations in the Earth-Moon system.

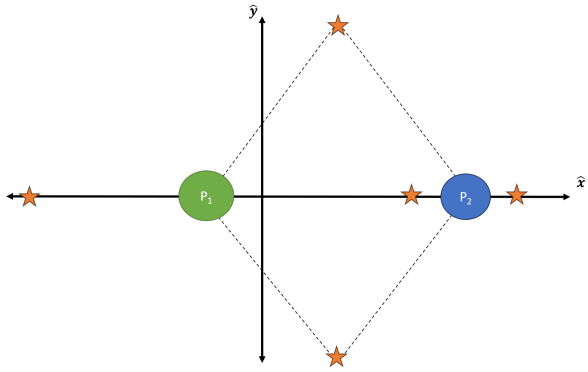

Figure 2.3. Equilibrium solutions in the CR3BP

One advantage of the simplified dynamics of the CR3BP is that it is a conservative system. As a result, a potential function can be written with a gradient equal to the equations of motion. This function and its gradient are formulated in the rotating frame rather than an inertial frame thus it is known as the pseudo-potential rather than a true gravitational

Table 2.1. Lagrange point locations in the Earth-Moon System

Point	x position (ND)	y position (ND)
L_1	0.8369	0
L_2	1.1559	0
L_3	-1.0051	0
L_4	0.4878	0.8660
L_5	0.4878	-0.8660

potential. Integrating the right hand side of Equations (2.12) to (2.14) with respect to x, y, and z respectively gives the pseudo-potential,

$$U^* = \frac{1-\mu}{d} + \frac{\mu}{r} + \frac{1}{2}(x^2 + y^2) \tag{2.24}$$

The equations of motion written in terms of the pseudo potential are

$$\begin{bmatrix} \ddot{x} \\ \ddot{y} \\ \ddot{z} \end{bmatrix} = \bar{\nabla} U^* + \begin{bmatrix} 2\dot{y} \\ -2\dot{x} \\ 0 \end{bmatrix} \tag{2.25}$$

Equation (2.25) are coupled and nonlinear, thus no analytic solution exists however the construction of the pseudo-potential allows for a better understanding of the behavior of the system.

Although there is no analytical solution to the CR3BP there is an integral of motion that can help characterize trajectories throughout the system. The integral of motion is a value calculated from state elements that does not change as the state is propagated in time. In the CR3BP the integral of motion is the Jacobi Constant. The constant is derived as follows. First, the dot product of Equation (2.25) with the velocity vector, $[\dot{x}, \dot{y}, \dot{z}]$, is computed as

$$\dot{x}\ddot{x} - 2\dot{x}\dot{y} + \dot{y}\ddot{y} + 2\dot{y}\dot{x} + \dot{z}\ddot{z} = \frac{\partial U^*}{\partial x}\dot{x} + \frac{\partial U^*}{\partial y}\dot{y} + \frac{\partial U^*}{\partial z}\dot{z} \tag{2.26}$$

The left hand side of Equation (2.26) is the dot product of velocity with acceleration as evident by the following

$$\dot{\bar{r}} \cdot \ddot{\bar{r}} = \dot{x}\ddot{x} + \dot{y}\ddot{y} + \dot{z}\ddot{z} \tag{2.27}$$

Notice the right hand side of Equation (2.26) is the total derivative of the pseudo-potential with respect to time. Therefore, the pseudo-potential is related to the dot product of velocity and acceleration by

$$\dot{\bar{r}} \cdot \ddot{\bar{r}} = \frac{dU^*}{dt} \tag{2.28}$$

This relation can then be integrated in terms of t producing

$$\frac{1}{2}(\dot{x}^2 + \dot{y}^2 + \dot{z}^2) = U^* + constant \tag{2.29}$$

Rearranging and redefining the arbitrary integration constant leads to the final equation for the Jacobi Constant expressed as

$$JC = 2U^* - V^2 \tag{2.30}$$

The Jacobi Constant, denoted as JC, acts as an energy-like quantity that does not change along an individual arc propagated through the CR3BP dynamics.

2.2 CR3BP + low thrust

Low thrust is augmented to the CR3BP to model the behavior of a spacecraft undergoing forces from two gravitational bodies and a low thrust engine. If the engine is producing an acceleration of $\bar{T} = [T_x, T_y, T_z]$, expressed in rotating coordinates, at an instant in time then the new equations of motion governing the behavior of the spacecraft at that moment are given by

$$\ddot{x} = 2\dot{y} + x - \frac{(1-\mu)(\mu+x)}{d^3} - \frac{\mu(x-1+\mu)}{r^3} + T_x \tag{2.31}$$

$$\ddot{y} = -2\dot{x} + y - \frac{(1-\mu)(y)}{d^3} - \frac{\mu y}{r^3} + T_y \tag{2.32}$$

$$\ddot{z} = -\frac{(1-\mu)(z)}{d^3} - \frac{\mu z}{r^3} + T_z \tag{2.33}$$

These equations assume the spacecraft mass remains fixed throughout the thrust arc. This assumption reduces the dimension of the problem by removing the need for an equation for mass change rate. Additionally, it underestimates engine performance and has been demonstrated by Cox to give useful insights into the transfer design process with very little change in geometry from the variable mass model [27].

There are several options for selecting the thrust vector, $\bar{T}$, with different advantages and drawbacks. Later sections select the thrust vector through optimization, however it is difficult to gain an understanding of the effects a specific thrust vector has at a particular time through these methods. Often the low thrust effect on Jacobi Constant is of particular concern when constructing transfers. To gain insights into the effect on the Jacobi Constant due to low thrust, the derivative of the Jacobi Constant with respect to time is computed as presented in

$$\frac{dJC}{dt} = -2\dot{x}U_x^* - \dot{y}U_y^* - 2\dot{z}U_z^* \tag{2.34}$$

In the ballistic equations of motion the derivative equals zero by construction, however with the augmented low thrust equations of motion the derivative has extra low thrust terms given by

$$\frac{dJC_{LT}}{dt} = \frac{dJC}{dt} - 2\dot{x}T_x - \dot{y}T_y - 2\dot{z}T_z \tag{2.35}$$

The derivative is integrated to produce the total change in Jacobi Constant as in

$$\int \frac{dJC_{LT}}{dt}dt = \Delta JC_{LT} = -2\int \dot{x}T_x + \dot{y}T_y + \dot{z}T_z dt \tag{2.36}$$

Notice the terms within the integral of Equation (2.36) are the dot product of velocity and thrust as expressed below.

$$\Delta JC_{LT} = -2\int \bar{v}\cdot\bar{T}dt \tag{2.37}$$

Equation (2.37) has three important implications. First, the Jacobi Constant is changed most efficiently when thrusting occurs while the spacecraft has the highest velocity in the rotating frame. Second, the greatest change in Jacobi Constant occurs when thrust is aligned with the spacecraft velocity in the rotating frame. Third, the negative sign at the beginning of the

expression indicates that thrusting in the velocity direction decreases the Jacobi Constant while thrusting in the anti-velocity direction increases it.

2.2.1 Inertially Fixed Thrust Vector

In transfer design applications it is important to consider the restrictions imposed by hardware. Most spacecraft cannot continuously vary their thrust vector. As a result, an understanding of an inertially fixed thrust vector low-thrust model is necessary for practical transfer design. A thrust vector fixed in the inertial frame is transformed into rotating frame coordinates and added to the CR3BP equations of motion. The resulting equations describe the motion of a spacecraft in cislunar space thrusting in a fixed direction. The first step in producing the equations of motion is to define the direction cosine matrix used for the frame rotation.

Consider an arbitrary inertial frame centered at the system barycenter with a Z axis aligned with the rotating frame z axis. At an arbitrary time t_0 the rotating frame x and y axes are aligned with the inertial X and Y axes respectively. As previously stated the rotation rate of the frame in nondimensional units is 1. Therefore the equation

$$\theta = n(t - t_0) = t - t_0 \tag{2.38}$$

represents the angle between the frames as a function of time. The Direction Cosine Matrix (DCM) based on this angle is used to rotate a thrust vector in the inertial frame to the rotating frame. The DCM is of the following form.

$$\bar{T}^R = \begin{bmatrix} cos(t-t_0) & sin(t-t_0) & 0 \\ -sin(t-t_0) & cos(t-t_0) & 0 \\ 0 & 0 & 1 \end{bmatrix} \bar{T}^I \tag{2.39}$$

The inertially fixed thrust vector in rotating coordinates is added to the CR3BP equation of motion to define the new inertially fixed thrust equations of motion,

$$\ddot{x} = 2\dot{y} + x - \frac{(1-\mu)(\mu+x)}{d^3} - \frac{\mu(x-1+\mu)}{r^3} + T_x^I cos(t-t_0) + T_y^I sin(t-t_0) \tag{2.40}$$

$$\ddot{y} = -2\dot{x} + y - \frac{(1-\mu)(y)}{d^3} - \frac{\mu y}{r^3} - T_x^I sin(t-t_0) + T_y^I cos(t-t_0) \tag{2.41}$$

$$\ddot{z} = -\frac{(1-\mu)(z)}{d^3} - \frac{\mu z}{r^3} + T_z^I \tag{2.42}$$

Notice Equations (2.40) to (2.42) explicitly depend on time and therefore no constant integral of the motion exists for this mathematical model.

2.2.2 Propellant Cost

Comparing low thrust transfers with impulsive ΔV transfers is not straight forward. Often total ΔV is used to define the cost of a transfer however this method fails to account for the added efficiency of low thrust engines. The main advantage of low thrust is how little propellant mass is required to produce a ΔV. The efficiency metric for the propellant cost is specific impulse (I_{sp}). Low thrust engines generally use electric propulsion to produce thrust rather than the chemical reactions in near impulsive engines. Table 2.2 gives an overview of several types of low thrust propulsion mechanisms as well as a conventional chemical engine for comparison [30][31][32][33].

Table 2.2. Performance of various spacecraft propulsion systems

System	Thrust Magnitude Range (mN)	ISP (s)	Technology readiness
Electro Static Ion Thrusters	25-300	2000-10,000	Flight Proven
Hall Effect Thrusters	40-600	1000-8000	Flight Proven
Solar Sails	$.00908/m^2$ (at 1 AU)	∞	Flight Proven
Field Emission Electric Propulsion	.0001-1.2	7000-11,000	Under development
Chemical rockets	2e5-4e5	100-400	Flight Proven

The low thrust engines can have I_{sp} an order of magnitude higher than that of nearly impulsive engines. This added efficiency results in lower propellant mass requirements for transfers. The transfers computed in Chapter 6 are compared to impulsive transfers from the literature as well as the Theoretical Minimum ΔV (TMDV). In order to make this comparison the rocket equation converts the ΔV to a required propellant mass. The comparison of propellant requirements is more illustrative of the real cost of these trajectories and acknowledges the advantage of the higher I_{sp} propulsion systems. The rocket equation[26] is formulated as follows,

$$\Delta m = m_0(1 - \mathrm{e}^{\frac{\Delta V}{g_0 I_{sp}}}) \tag{2.43}$$

For low thrust transfers rather than calculate a ΔV, the time history of the thrust magnitude, $\bar{T}(t)$, is converted to propellant requirements directly. This relation is

$$\Delta m = \int \frac{T m_0}{g_0 I_{sp}} dt \tag{2.44}$$

These equations are used to compute the propellant mass required for orbital transfers, thus allowing for a consistent comparison between methods.

3. DYNAMIC SYSTEMS THEORY

Many numerical and analytical tools are used throughout this investigation to gain information about trajectories and other dynamic structures as well as their stability and sensitivities. The CR3BP has no analytical solution, therefore Dynamic Systems Theory (DST) is used to develope an understanding of the natural flow through the system. Throughout this chapter DST provides information about linear dynamics around arbitrary trajectories and periodic orbits. Differential corrections schemes are discussed and applied to the construction of periodic orbits, orbit stability is characterized and leveraged in the creation of global manifolds, and stretching directions are computed to produce quick departures from stable orbits. These techniques offer insights into the coupled non-linear dynamics of the CR3BP without the need for an analytical solution.

3.1 Linearization

The first step in understanding the cislunar environment is the linearization of the dynamics around equilibrium points. The linearization provides an estimate of the flow near the dynamically rich regions of the mathematical model. The linearization process begins with a state near an equilibrium point. The position of the state relative to the equilibrium point can be written as $\tilde{x} = [\xi, \eta, \zeta]$. The linearized equations of motion are given by

$$\ddot{\xi} = 2\dot{\eta} + \frac{d^2U^*}{dx^2}\xi + \frac{d^2U^*}{dxdy}\eta + \frac{d^2U^*}{dxdz}\zeta \tag{3.1}$$

$$\ddot{\eta} = -2\dot{\xi} + \frac{d^2U^*}{dydx}\xi + \frac{d^2U^*}{dy^2}\eta + \frac{d^2U^*}{dydz}\zeta \tag{3.2}$$

$$\ddot{\zeta} = \frac{d^2U^*}{dzdx}\xi + \frac{d^2U^*}{dzdy}\eta + \frac{d^2U^*}{dz^2}\zeta \tag{3.3}$$

where, ξ refers to the x distance from the Lagrange point, η refers to the y distance from the lagrange point, and ζ refers to the z distance from the lagrange point. The first derivative of the equations of motion around the equilibrium point acts as a linear estimate for nearby relative motion.

Equations (3.1) to (3.3) constitute a linear approximation of the behavior of trajectories near equilibrium points. As a result they are only valid relatively close to the point of interest. The equations are written in matrix form as

$$\dot{\tilde{x}} = A\tilde{x} \tag{3.4}$$

where

$$A = \begin{bmatrix} 0 & 0 & 0 & 1 & 0 & 0 \\ 0 & 0 & 0 & 0 & 1 & 0 \\ 0 & 0 & 0 & 0 & 0 & 1 \\ U^*_{xx} & U^*_{xy} & U^*_{xz} & 0 & 2 & 0 \\ U^*_{xy} & U^*_{yy} & U^*_{yz} & -2 & 0 & 0 \\ U^*_{xz} & U^*_{yz} & U^*_{zz} & 0 & 0 & 0 \end{bmatrix} \tag{3.5}$$

The resulting linear system is analyzed through conventional techniques to give insights into the more complex non-linear dynamics.

The linear system can be solved by reducing the space into an eigendecomposition. Any solution can be written as a summation of the eigenmodes of the system represented below

$$\tilde{x}(t) = \sum c_{\mathrm{i}} \mathrm{e}^{\lambda_{\mathrm{i}} t} \bar{v}_{\mathrm{i}} \tag{3.6}$$

In Equation (3.6) λ_{i} are the eigenvalues and $\bar{v}_{\mathrm{i}}$ are the associated eigenvectors of the A matrix. The specific relative state of interest results in different constants, c_{i}. The eigenvalues give fundamental information about the motion of trajectories near the equilibrium points. The growth and decay of perturbations from an equilibrium point is determined by the real part of the eigenvalues. Unstable motion is indicated by $\mathrm{Re}(\lambda) > 0$. A perturbation in the eigenvector associated with this eigenvalue asymptotically departs the area. Stable motion is indicated by $\mathrm{Re}(\lambda) < 0$. A trajectory exciting this vector asymptotically approaches the equilibrium point. Lastly, $\mathrm{Re}(\lambda) = 0$ indicates marginally stable motion. In a linear sense these trajectories stay the same distance from the equilibrium points however, non-linear

dynamics may perturb the trajectory in some other direction over larger integration times. The eigenvalues of the equilibrium points in the Earth-Moon system are given in Table 3.1.

Table 3.1. Eigenvalues associated with linear motion about each equilibrium point in the Earth-Moon CR3BP

Point	λ_1	λ_2	λ_3	λ_4	λ_5	λ_6
L1	2.9321	-2.9321	2.3344i	-2.3344i	2.2689i	-2.2689i
L2	2.1586	-2.1586	1.8626i	-1.8626i	1.7862i	-1.7862i
L3	0.1779	-0.1779	1.0104i	-1.0104i	1.0053i	-1.0053i
L4	0.9545i	-0.9545i	0.2982i	-0.2982i	1.0000i	-1.0000i
L5	0.9545i	-0.9545i	0.2982i	-0.2982i	1.0000i	-1.0000i

Just as the linear dynamics give information about trajectories near the equilibrium points, another linearization produces information about trajectories near some reference trajectory. This linearization is known as the State Transition Matrix (STM). Consider a trajectory, $\bar{x}(t)$, near some reference trajectory, $\bar{x}^*(t)$. These trajectories are related by

$$\bar{x}(t) = \bar{x}^*(t) + \delta\bar{x}(t) \tag{3.7}$$

The time derivative of Equation (3.7) is computed to produce

$$\dot{\bar{x}} = \dot{\bar{x}}^* + \delta\dot{\bar{x}} = \bar{f}(\bar{x}^* + \delta\bar{x}, t) \tag{3.8}$$

Then, a first order Taylor expansion about $\dot{\bar{x}}^*(t)$ is computed to estimate the motion of $\dot{\bar{x}}(t)$. This expansion is then truncated to only include linear terms resulting in

$$\dot{\bar{x}} \approx \bar{f}(\bar{x}^*, t) + \frac{\partial \bar{f}}{\partial \bar{x}}\delta\bar{x} \tag{3.9}$$

Replacing the left hand side of Equation (3.9) with Equation (3.8) and subtracting the original solution, $\dot{\bar{x}}^*$ from both sides produces the first order approximation of the variation in the solution. The equation is given by

$$\delta\dot{\bar{x}} = \frac{\partial \bar{f}}{\partial \bar{x}}\delta\bar{x} \tag{3.10}$$

Equation (3.10) gives the derivative of the change in state of a nearby trajectory relative to the reference trajectory. The partial derivative matrix is the same linearization matrix, A, used to estimate motion near equilibrium points. However, A is a function of time along the reference trajectory rather than a constant matrix. The initial value of the state variation is the identity matrix. It is integrated forward in time along the reference trajectory using Equation (3.10) to produce the STM along the reference. The STM for a trajectory beginning at time t_0 and ending at time, t is denoted by $\Phi(t, t_0)$. It is applied to any relative state to give a linear estimate of that relative state at some time, t, along the trajectory as .

$$\delta\bar{x}(t) = \Phi(t, t_0)\delta\bar{x}(t_0) \tag{3.11}$$

Some useful propreties of the STM are listed below

$$\Phi(t_2, t_0) = \Phi(t_2, t_1)\Phi(t_1, t_0) \tag{3.12}$$

$$\Phi(t_0, t_1) = \Phi^{-1}(t_1, t_0) \tag{3.13}$$

The STM is a powerful tool in DST. It is used throughout this investigation to estimate sensitivities, understand the stability of orbits, and compute stretching directions. These applications are discussed in later sections of this chapter.

3.2 Differential Corrections

Targeting methods are commonly used in trajectory design problems. In multi-body applications it is often desirable to select a trajectory that approximates a dynamic structure. This may be searching for an orbit, a manifold, a transfer, or some other criteria. Additionally, constraints such as energy level, periodicity, perpendicular crossings, and thrust constraints are often added to ease the targeting process or meet the needs of the mission. A set of free variables is selected to meet all these criteria and the differential corrector can iteratively adjust the free variables to select values that meet all the constraints within some preset tolerance level. A Newton-Raphson targeting scheme is used in this investigation due

to its efficient quadratic convergence. The limitation of Newton-Raphson is that the partial derivatives of all the constraint functions with respect to each of the free variables is required. Given a guess of the free variable vector written as

$$\bar{X} = \begin{bmatrix} X_1 \\ X_2 \\ \vdots \\ X_n \end{bmatrix} \tag{3.14}$$

and constraints written as

$$\bar{F}(\bar{X}) = \begin{bmatrix} F_1(\bar{X}) \\ F_2(\bar{X}) \\ \vdots \\ F_n(\bar{X}) \end{bmatrix} \tag{3.15}$$

the update equation is as follows

$$\bar{X}_{\mathrm{i}+1} = \bar{X}_{\mathrm{i}} - DF(\bar{X}_{\mathrm{i}})^{-1}\bar{F}(\bar{X}_{\mathrm{i}}) \tag{3.16}$$

Equation (3.16) produces an updated free variable vector that is closer to the solution then the previous, provided that the initial guess is sufficiently close for convergence. The DF matrix, often denoted as the Jacobian, contains the derivatives of the target functions with respect to the free variables. Each row of the matrix gives derivatives of a particular function while each column is with respect to a particular variable.

3.2.1 Single Shooter

The simplest implementation of the targeting scheme is the single shooter. In this method the free variables are elements of a single propagated arc through the system. Single shooting is usually sufficient for targeting with relatively low sensitivity and shorter times of flight. In this investigation the single shooter is used to construct libration point orbits in the CR3BP

that are used as initial and final locations for transfers. The construction of these orbits is discussed more in section 3.4.

For a simple single shooter example a single arc is propagated in the CR3BP. The initial velocity is then changed slightly via the newton-rhapson update equation to calculate a new initial velocity. The goal of this example targeting process is to select a velocity at the initial state that creates a trajectory with a particular final position. Notice that the system is square as three initial state elements are free and three final state elements are constraints. The DF matrix for this example is

$$DF = \begin{bmatrix} \phi_{14} & \phi_{15} & \phi_{16} \\ \phi_{24} & \phi_{25} & \phi_{26} \\ \phi_{34} & \phi_{35} & \phi_{36} \end{bmatrix} \tag{3.17}$$

where, ϕ represents the elements of the STM with the first subscript identifying the row and and the second the column.

Figure 3.1 depicts the trajectories at each iteration of the targeting process. The error at each iteration is shown in Figure 3.2. Notice, the quadratic convergence indicating the STM is acting as a good approximation for the state derivatives. However, STMs of longer trajectories contain less accurate approximations of the state sensitivities. A single shooter method for these longer trajectories takes more iterations to converge and at times may not converge at all. Therefore, the single shooting method is only implemented for relatively short trajectories.

3.2.2 Multiple Shooter

Often the single shooter scheme is not sufficient for the sensitivity of transfers between orbits. Trajectories with close lunar approaches or long times of flight also increase the sensitivity of the problem. In these cases a multiple shooter is necessary. The multiple shooter, propagates several arcs with continuity constraints between each to create a single trajectory. The build up of integration error is notably reduced by splitting the trajectory into multiple arcs. Additionally, the lower magnitudes of STM elements improves the accuracy

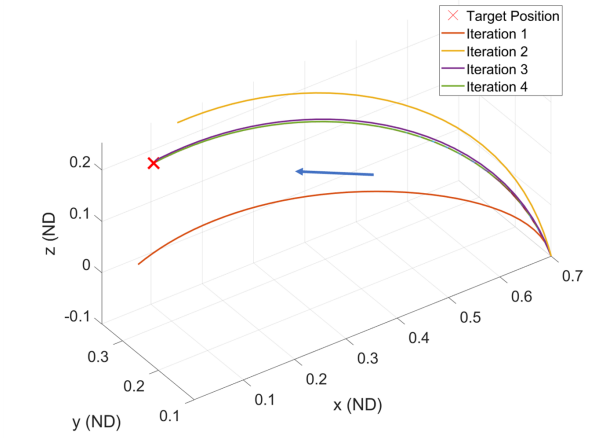

Figure 3.1. Trajectories at each iteration of the single shooter position targeting problem

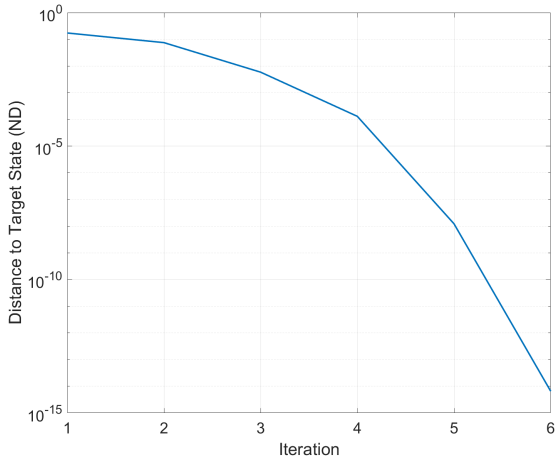

Figure 3.2. Distance from trajectory end state to target state at each iteration of the targeting process

of th matrix inversion in Equation (3.16). The linear estimation of the STM is also more accurate for shorter propagation times. Figure 3.3 shows a schematic of the multiple shooter arcs.

The main challenge present when implementing a multiple shooter is that it notably increases the dimension of the problem. In the ballistic case the addition of 1 extra arc increase the free variables and target functions by six. In the Indirect optimization case the dimension is increase by twelve per arc due to the addition of costate elements along

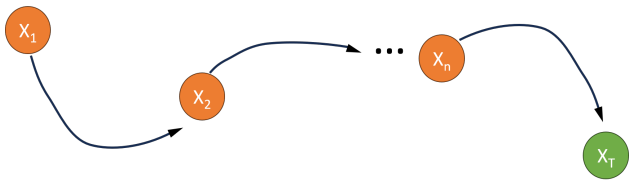

Figure 3.3. Diagram of a multiple shooting method

each trajectory as discussed further in section 4.1. Therefore the method is only used when sensitivity requires it.

3.3 Parameter Sensitivities

In transfer design problems targeting schemes often require the derivative of a final state of a trajectory with respect to the change in a system parameter. Specifically, the targeting process for low-thrust transfers may employ the sensitivity of the trajectory final states with respect to a thrust vector. The sensitivity of a state due to a changing parameter is not calculated by the STM discussed in the previous section. As a result, a new method for computing the sensitivity of a parameter is required. This method is derived in the following section.

Similar to the STM the time derivative of the sensitivity is calculated at each point along a trajectory. The derivation is integrated along with the trajectory to produce the partial derivative of the final state with respect to the parameter. Therefore, the value $\frac{d}{dt}(\frac{d\bar{x}}{dT})$ is required to compute $\frac{d\bar{x}}{dT}$[34]. The first step in calculating this quantity is to reverse the order of derivation. Recall the quantity $\frac{d\bar{x}}{dt}$ is already defined by the equations of motion in the CR3BP denoted as f. The derivative is therefore written as

$$\frac{d}{dt}(\frac{d\bar{x}}{dT}) = \frac{d}{dT}(\frac{d\bar{x}}{dt}) = \frac{d}{dT}(\bar{f}) \tag{3.18}$$

Thus, the sensitivity with respect to the parameter T is the total derivative of the equations of motion with respect to T as in the right hand side of Equation (3.18). The differential equation for computing this quantity is

$$\frac{d}{dt}(\frac{d\bar{x}}{dT}) = \frac{d\bar{f}}{d\bar{x}}\frac{d\bar{x}}{dT} + \frac{d\bar{f}}{dT} \tag{3.19}$$

by the chain rule. The sensitivity derivative is propagated along the trajectory of interest to produce the sensitivity at the final state. Changing a model parameter has no effect on the initial state of a trajectory, thus the initial sensitivity is zero. The formulation of the parameter sensitivity informs targeting problems that have thrust as a free variable such as the inertially fixed thrust transfer targeter discussed in Chapter 5.

3.4 Periodic Orbits

The key to understanding dynamic systems is computing and understanding periodic orbits. A periodic orbit is a solution within the dynamics that returns to an initial point after some period of time, P, known as the orbital period. This definition is given as

$$\gamma(t + P) = \gamma(t) \tag{3.20}$$

The CR3BP does not have an analytical solution thus orbits must be computed numerically. Different methods of construction are used depending on the symmetry of the orbits. For asymmetric orbits the initial and final point of an arc are constrained to match in full six dimensional space to within some tolerance level. However, the symmetry of the system discussed in section 2.1 often allows for simpler computation. For symmetric orbits, half of the orbit is computed ensuring it begins and ends with a perpendicular crossing of the x-z plane. This perpendicular crossing constraint results in the symmetric solution closing the curve and creating a periodic orbit. Targeting this orbit requires the initial and final points

on the trajectory to have a value of 0 for the y, $\dot{x}$, and $\dot{z}$ elements. The targeting problems for symmetric and asymmetric orbits are

$$\bar{X} = \begin{bmatrix} x_0 \\ z_0 \\ \dot{y}_0 \end{bmatrix}, \bar{F} = \begin{bmatrix} y_f \\ \dot{x}_f \\ \dot{z}_f \end{bmatrix} \tag{3.21}$$

$$\bar{X} = \begin{bmatrix} y_0 \\ z_0 \\ \dot{x}_0 \\ \dot{y}_0 \\ \dot{z}_0 \end{bmatrix}, \bar{F} = \begin{bmatrix} x_f - x_0 \\ y_f - y_0 \\ z_f - z_0 \\ \dot{x}_f - \dot{x}_0 \\ \dot{y}_f - \dot{y}_0 \end{bmatrix} \tag{3.22}$$

Equations (3.21) and (3.22) represent fixed period targeting schemes however integration time can be added to the free variables with the removal of a state element to produce variable time targeters.

Notice only five state elements are constrained in the asymmetric problem. The final element is implicitly constrained by the Jacobi Constant, therefore the five dimensional constraint vector sufficient to ensure six dimensional convergence. These targeting methods produce the orbits that are used for transfers in Chapter 6. The asymmetric orbits of interest are the L_4 Short Period Orbits (L4SPO). The initial guess for generating these orbits is constructed from the in-plane short period marginally stable mode of the L_4 lagrange point. Additionally, several transfers between symmetric orbits are constructed. These orbits include Distant Retrograde Orbits (DRO), and both L_1 and L_2 halo orbits. The initial guess for the DROs is based on a two-body circular retrograde orbit about the Moon, while the halo orbits are constructed from a bifurcation off of the L_1 and L_2 lyapunov families. A more complete discussion of periodic orbit family generation is available by Grebow[35]. Subsections of the L_1 lyapunovs, L_1 halos, L4SPOs and DROs are shown in Figures 3.4 to 3.7.

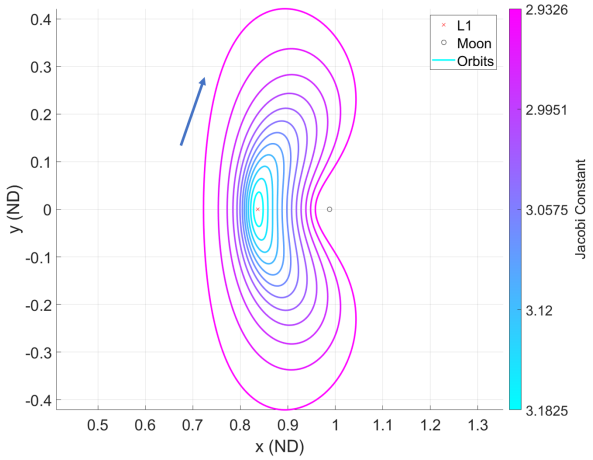

Figure 3.4. A section of the L1 lyapunov orbits in the Earth-Moon System

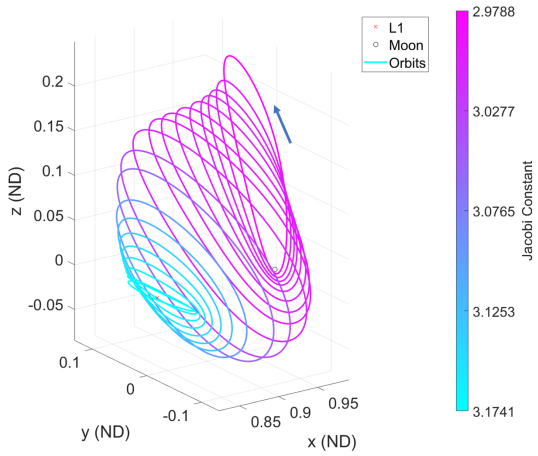

Figure 3.5. A section of the L1 northern halo orbits in the Earth-Moon System

3.5 Stability of Periodic Orbits

The periodic orbits are analyzed in terms of their linear stability using similar methods as those employed for lagrange points. A new stability condition based on Floquet theory is introduced for characterizing periodic orbits. First consider a point along the periodic orbit. Propagating this point for exactly one period results in the trajectory returning to the original location, thus the point is denoted a fixed point. The STM propagated with the

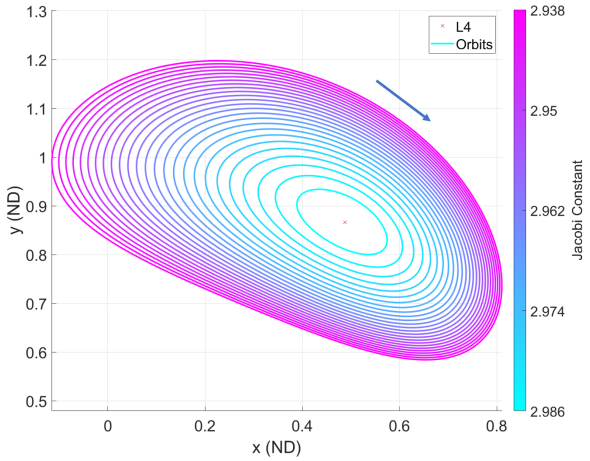

Figure 3.6. A section of the L4 short period orbits in the Earth-Moon System

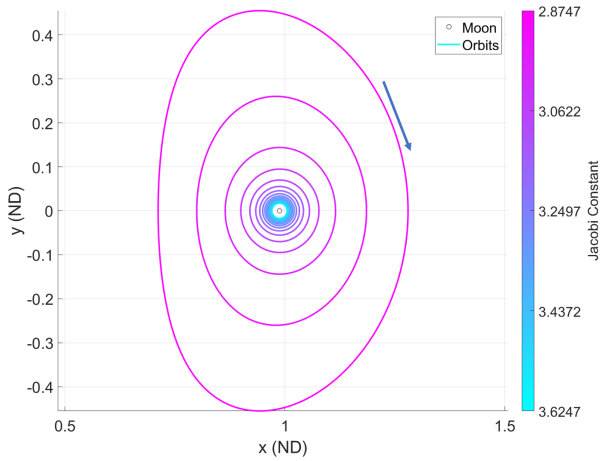

Figure 3.7. A section of the distant retrograde orbits in the Earth-Moon System

fixed point for one orbit is known as the monodromy matrix. From Floquet's theorem the eigenstructure of the monodromy matrix describes the stability of the periodic orbit[36].

The eigenvlaues predict the behavior of a state perturbed off the fixed point as it is propagated for one orbital period. As with the equilibrium points, these predictions are linear in nature and are therefore only valid for states relatively close to the fixed point. Unlike the equilibrium points the predictions are produced based on discrete applications of the monodromy matrix rather than a continuous application of the equations of motion. The new stability criteria are as follows[19].

- **Unstable Eigenvalues:** if $|\lambda_i| > 1$, then the eigenvalue is unstable. Perturbations that excite this eigenvalue will grow in forward time.
- **Stable Eigenvalues** if $|\lambda_i| < 1$, then the eigenvalue is stable. Perturbations that excite this eigenvalue will decay in forward time.
- **Marginally Stable Eigenvalues** if $|\lambda_i| = 1$, then the eigenvalue is marginally stable. Perturbations that excite this eigenvalue will remain the same magnitude in forward time.

The autonomous nature of the CR3BP ensures that the eigenvalues of the monodromy matrix occur in reciprocal pairs. This is due to Lyapunov Theorem stated as

Theorem 3.5.1. *if λ is an eigenvalue of the monodromy matrix $\Phi(t_0 + P, t_0)$ of a time invariant system, then λ^{-1} is also an eigenvalue, with the same structure of elementary divisors.*

There are six directions a state can be perturbed relative to a fixed point. One of the directions simply moves th state along the orbit. Propagating this stepped state for one period results in it returning to the exact same location. Therefore their must be an eigenvector in the orbital direction with an associated eigenvalue of unity. The unity eigenvalue represents additional fixed points along the orbit. All monodromy matrices in th CR3BP must have an eigenvalue of unity because any point along the orbit can act as a fixed point. Theorem 3.5.1 therefore guarantees a second unity eigenvalue, implying that all periodic orbits in the system must exist within continuous families as perturbations in th direction associated with this second unity eignvalue must also return to the same location.

An orbit is considered unstable if at least 1 of its eignvalues is unstable. Due to Theorem 3.5.1 any orbit with stable eigenvalues must also have unstable eigenvalues. Consequently, no stable orbits can exist in the CR3BP. However, many orbits have all six of their eigenvalues on the unit circle indicating marginal stability. Other orbits such as the 9:2 NRHO have very small unstable eigenvalues that means perturbations take a significant amount of time to grow resulting in very slow natural departure or arrival on to the orbit. In order to quantify the stability of an orbit a stability metric is defined.

Many different stability index definitions exist for orbits in the CR3BP. For this investigation the stability index determines whether stable and unstable manifolds exist for a particular orbit. The infinity norm of the eigenvalues associated with a monodromy matrix is a sufficient stability index for this application. This definition of stability index is represented as

$$SI = |\bar{\lambda}|_\infty \tag{3.23}$$

Any orbit with a stability index greater than 1 is unstable and therefore has stable and unstable manifolds that can be leveraged for transfer construction. Orbits with a stability index of 1 are marginally stable and therefore lack stable and unstable manifolds. Transfers involving marginally stable orbits are constructed using stretching directions. Orbit manifolds are discussed more in depth in the next section while stretching directions are discussed in section 3.8.

3.6 Invariant Manifold Theory

Invariant manifolds are an import structure in traversing cislunar space. One of the goals of this investigation is to move between orbits as efficiently as possible. Efficiency in the form a propellant savings is facilitated by leveraging the the natural flow of the CR3BP. This natural flow is governed by manifolds. The unstable manifold represents maneuver free departure from an unstable orbit, while the stable manifold represents free arrival on an unstable orbit. The construction of these manifolds and their characteristics is presented in this section.

3.6.1 Invariant Subspaces

Consider a fixed point on a periodic orbit with eigenvectors of the monodromy matrix, $\bar{v}_{\text{i}}$. The 6 dimensional space surrounding the point is represented in terms of fundamental subspaces spanned by the eigenvectors as

$$\mathbb{R}^6 = E^S + E^U + E^C \tag{3.24}$$

Here the superscripts represent the fundamental motion of the the subspace; E^S is stable, E^U is unstable, and E^C is the center subspace. These subspaces are invariant under the linear dynamics of the region. The invariance guarantees that a state within a subspace remains within the subspace when the linear dynamics of the monodromy matrix are applied.

3.6.2 Local Manifolds

The linear invariant subspaces are generalized to form local manifolds within the non-linear system dynamics. According to the stable manifold theorem of periodic orbits[37], if there is an m dimensional linear stable subspace associated with a point on an orbit then there exists an $m+1$ dimensional local stable manifold, W^S_{loc}, that is invariant under the non-linear dynamics. This manifold is tangent to the stable subspace at all points along the orbit and asymptotically approaches the orbit as $t \to \infty$. Analogously, if there is a k dimensional linear unstable subspace associated with the point, then there exists a $k+1$ dimensional local unstable manifold, W^U_{loc}. This manifold is tangent to E^U at all points along the orbit and asymptotically approaches the orbit as $t \to -\infty$. A diagram of the relationship between the linear subspace and local manifold appears in Figure 3.8

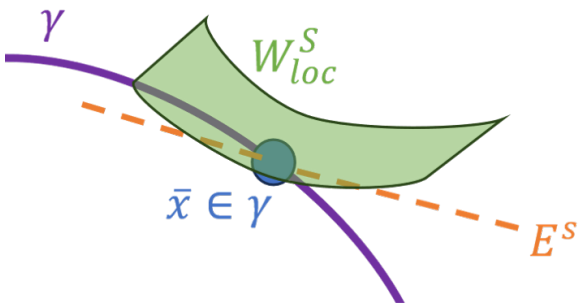

Figure 3.8. Diagram of the relationship between linear and local nonlinear manifolds of a fixed point

3.6.3 Global Manifolds

The local manifolds are expanded to the full non-linear manifolds of the orbit to gain a greater understanding of the flow throughout the system. These manifolds span the cislu-

nar region and govern motion in forward and backward time. In this subsection the local manifolds are used to construct the full global manifolds that are used as initial guesses for transfers in Chapter 6. The tangency condition described in the previous subsection is leveraged to begin constructing the global manifolds. A point approximately on the local manifold is produced by stepping a small distance, β, from a fixed point in the direction of the stable or unstable subspace. Both halves of the manifold are produced by stepping in the positive and negative eigenvector directions. Construction of points on both halves of the stable and unstable manifolds are given by

$$\bar{x}_S^+ = \gamma + \beta \bar{v}_S \tag{3.25}$$

$$\bar{x}_S^- = \gamma - \beta \bar{v}_S \tag{3.26}$$

$$\bar{x}_U^+ = \gamma + \beta \bar{v}_U \tag{3.27}$$

$$\bar{x}_U^- = \gamma - \beta \bar{v}_U \tag{3.28}$$

Selection of an appropriately sized β is challenging. The step size depends on the stability properties of the orbit as well as the μ value of the system. The invariant subspaces and local manifolds are only tangent at the underlying fixed point. As a result, too large a step size results in a poor approximation of a point on the manifold. However, too small a step size results in a point that when propagated takes a long time to leave the vicinity of the orbit. This added propagation time can create additional unnecessary numerical error build up.

Points on the local manifold are computed from several points around the periodic orbit. Each point is then propagated forward in time for the unstable manifold or backward in time for the stable manifold. The resulting trajectories are approximately on the stable and unstable manifolds of the orbit. An example of trajectories on the manifolds of a lyapunov orbit is shown in Figure 3.9. In this depiction the manifolds are propagated to fixed x locations, however greater coverage of the cislunar region is possible through longer propagation times.

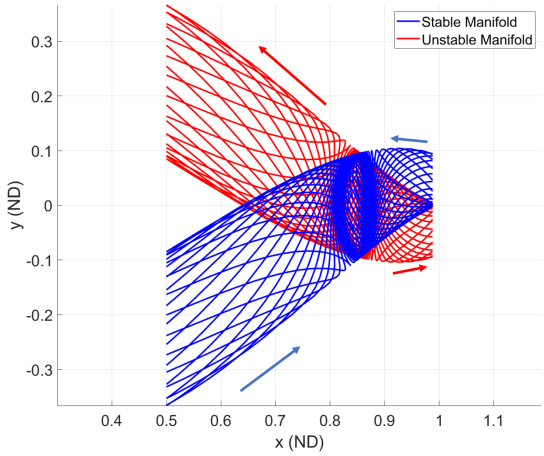

Figure 3.9. Manifolds of an L1 lyapunov orbit, JC = 3.15

3.7 Theoretical Minimum Delta V

Transfers are not limited to orbits of the same energy level. In astrodynamic applications, spacecraft often need to bridge an energy gap when moving between orbits. Any transfer between orbits of different Jacobi Constants must expend propellant to overcome the difference in energy. The Theoretical Minimum ΔV (TMDV) acts as a metric for the cost to change a trajectories energy. The TMDV provides a benchmark for how large a maneuver is necessary to change the energy of a trajectory depending on the initial and final Jacobi Constant as well as the location the maneuver takes place. This metric can be converted to a propellant cost using Equation (2.43).

Consider two trajectories with Jacobi Constants of JC_1 and JC_2. These values are written out in terms of their velocity and pseudo potential as

$$JC_1 = 2U_1^* - V_1^2 \tag{3.29}$$

$$JC_2 = 2U_2^* - V_2^2 \tag{3.30}$$

Thus the change in JC is expressed as

$$JC_2 - JC_1 = 2(U_2^* - U_1^*) - (V_2^2 - V_1^2) \tag{3.31}$$

The ΔV must occur when the trajectories coincide in position, therefore $U_1^* = U_2^*$ and the first term of Equation (3.31) is 0. The second term in the equation is broken down as a difference of squares. Performing these simplifications and solving for ΔV results in

$$\Delta V = \frac{-\Delta JC}{(V_2 + V_1)} \tag{3.32}$$

Equation (3.32) provides similar insights into the effect on Jacobi Constant of a maneuver as Equation (2.37). First, the negative sign indicates that increasing velocity results in a decrease in Jacobi constant. Secondly, the denominator indicates that the TMDV is smaller when both trajectories are moving quickly and larger when moving slowly. This is equivalent to the low thrust result that Jacobi constant is changed most efficiently when spacecraft have a larger velocity when viewed in the rotating frame. The dependence on velocity implies for a particular energy change a different ΔV is required depending on the location the maneuver takes place. Trajectories have higher velocity in the rotating frame when near the primaries, resulting in lower TMDV in these regions. Figure 3.10 illustrates the TMDV for a transfer between trajectories at JC of 3.0 and 3.1 depending on the maneuver location in the planar problem.

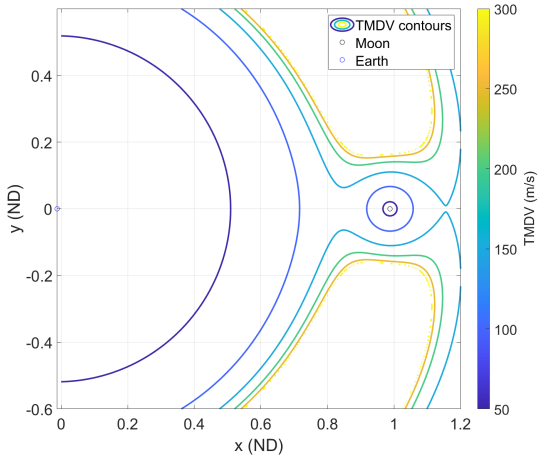

Figure 3.10. Map of TMDV for a transfer between orbits of JC = 3.0 and 3.1

3.8 Stretching Directions

The monodromy matrix is useful in identifying characteristic flow around a periodic orbit, however it cannot be applied to aperiodic trajectories. Information about behavior around arbitrary trajectories is captured by the stretching directions of the STM. Stretching directions are also useful when an orbit does not have an unstable manifold yet quick departure is desired. The stretching directions and singular values provide information about the change in magnitude of a variation from the reference trajectory over a specified time horizon[38]. The singular value decomposition of th STM is provided as

$$\Phi(t, t_0) = U\Sigma\Xi^T \tag{3.33}$$

The STM, $\Phi(t, t_0)$ is decomposed into singular vectors and singular values. As such the predictions made by the decomposition is only valid for the time horizon from t to t_0. The right singular vectors that define an initial perturbation direction are denoted as Ξ. A diagonal matrix, Σ, contains the singular values of the matrix. These values define how a perturbation in the associated right singular vector expands or contracts over the time horizon of interest. Values less than 1 are associated with contraction while values greater than 1 are associated with expansion. Lastly, U represents the left singular directions that give the final direction of the perturbation after propagation. If some state is in the direction of $\bar{\xi}_\mathrm{i}$ relative to the reference trajectory then after propagation for time, t, the final perturbed state is in the direction of $\bar{u}_\mathrm{i}$ with the magnitude scaled by σ_i as expressed below

$$\sigma_\mathrm{i}\bar{u}_\mathrm{i} = \Phi(t, t_0)\bar{\xi}_\mathrm{i} \tag{3.34}$$

Figure 3.11 visual represents this relation for a 2 dimensional case. In the diagram σ_1 is less than 1 while σ_2 is greater than 1.

Similar to the eigenvalues of the monodromy matrix the singular values of the STM define characteristic behavior of trajectories near the reference. sStretching and restoring subspaces are defined as

$$S^+ = span\{\xi_\mathrm{i}\}, \sigma_\mathrm{i} > 1 \tag{3.35}$$

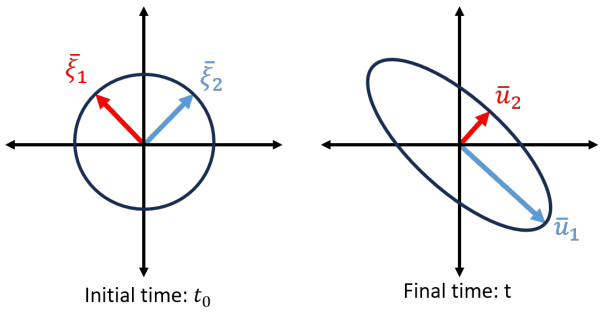

Figure 3.11. A 2D example of stretching directions and singular values over a specified time horizon

$$S^- = span\{\xi_i\}, \sigma_i < 1 \tag{3.36}$$

where, S^+ is a stretching subspace and S^- is a restoring subspace. Perturbations in a restoring subspace move closer to the reference after propagation over the time interval $[t_0, t]$, while perturbations in the stretching subspace move away[39].

There are a few key differences between the stretching direction and the eigendecomposition of the monodromy matrix that should be highlighted. First, the monodromy matrix only exists for periodic solutions. The advantage of applying periodic information is that the information is valid for an infinite time interval. The stretching directions on the other hand are applicable to any trajectory however they only give variational information for propagations over the same finite time span as the reference trajectory. Additionally, while the eigenspaces of the monodromy matrix are invariant, perturbations in a stretching direction change direction based on the left singular vectors. These directions are specific to a particular time interval. Both methods are based on linear approximations and therefore are not applicable for overly large perturbations.

An additional flexibility afforded by stretching directions is that they relate variations in subsets of the state elements rather than the full six dimensional state. Stretching directions are employed to understand the effects of variations in velocity to model maneuver options. Nearly impulsive engines can change the velocity of a spacecraft nearly instantaneously but not position. Therefore, a stretching direction that relates an initial velocity variation to a final state variation is useful for the transfer design process.

The velocity stretching directions are computed by first subdividing the STM into four sub-matrices relating initial variations with final variations. The subdivided STM is presented as

$$\Phi(t, t_0) = \begin{bmatrix} \phi_{rr} & \phi_{rv} \\ \phi_{vr} & \phi_{vv} \end{bmatrix} \tag{3.37}$$

where ϕ_{rr} represents the change in final position based on a change in initial position, ϕ_{rv} represents the change in final position based on a change in initial velocity, ϕ_{vr} represents the change in final velocity based on a change in initial position, and ϕ_{vv} represents the change in final velocity based on a change in initial velocity. The sub-matrix, $\phi_{rv,v} = \begin{bmatrix} \phi_{rv} \\ \phi_{vv} \end{bmatrix}$, describes the effects of an initial ΔV on a final state. The initial change in velocity is a three dimensional vector and the final change in state is a six dimensional vector. The singular values and directions for the change in initial velocity is as follows

$$\Phi_{rv,v} = U\Sigma\Xi^T \tag{3.38}$$

$$U = \begin{bmatrix} \bar{u}_1 & \bar{u}_2 & \bar{u}_3 & \bar{u}_4 & \bar{u}_5 & \bar{u}_6 \end{bmatrix} \tag{3.39}$$

$$\Sigma = \begin{bmatrix} \sigma_1 & 0 & 0 \\ 0 & \sigma_2 & 0 \\ 0 & 0 & \sigma_3 \\ 0 & 0 & 0 \\ 0 & 0 & 0 \\ 0 & 0 & 0 \end{bmatrix} \tag{3.40}$$

$$\Xi = \begin{bmatrix} \bar{\xi}_1 & \bar{\xi}_2 & \bar{\xi}_3 \end{bmatrix} \tag{3.41}$$

Analogous to the full state case singular values greater than 1 indicate growth over the time horizon of interest while singular values less than 1 indicate contraction. However by restricting the initial variation to velocity space the problem becomes over constrained. As indicated by the zeros in the second half of Σ the final directions $\bar{u}_4$, $\bar{u}_5$, and $\bar{u}_6$ are not influenced by the initial velocity change. Consequently, one disadvantage of only altering

the initial velocity is that their is a three dimensional subspace that cannot be accessed by velocity perturbed trajectories. The applications in hapter 6 do not require meeting a specific state, rather the velocity variations are used to form an initial guess trajectory that quickly leaves the orbit vicinity. Therefore, these limitations do not affect the analysis.

4. INDIRECT OPTIMIZATION

The addition of low-thrust terms into the CR3BP dynamics forms a continuously varying control problem for cislunar transfer applications. In this formulation each point in time has an associated three dimensional thrust vector. The added degrees of freedom notably expands the solution space of transfers between any two orbits. However, a method is needed to select an optimal transfer from the many alternatives. Functional optimization is employed to solve such problems where the input is a continuous time history rather than a discrete set of variables. There are several methods for solving these classes of problems but for this investigation indirect optimization is used based on the Calculus of Variation (CoV) to produce locally optimal solutions. The method converts the optimization problem into a 2 Point Boundary Value Problem (2PBVP) that is solved with the differential corrections techniques described in section 3.2 [40]. This section offers an overview of how CoV is used, however a more complete discussion of the methods and applications of the CoV is available by Bolza[41].

4.1 Euler Lagrange Theorem

The first step in the method is to determine the cost function denoted as J. The cost function must take in a function as an input, known as the control, $u(t)$, and output a single scalar value, J, that represents a cost. The goal of the optimization is to select a function $u(t)$ such that J is at a minimum. A general cost function is

$$J = J_{\mathrm{e}}(x_f, t_f) + \int L(x, t, u(t))dt \tag{4.1}$$

The cost consists of two terms. The first refers to the cost associated with the final state of the system and the second incorporates the cost along the path of the trajectory. The integrand L within Equation (4.1) is known as th Lagrangian and is generally a function of state, time, and the control input, $u(t)$. The goal of the CoV is to define criteria for the control that guarantees J is minimized. This criteria generally comes in the form of a differential equation for the evolution of $u(t)$ over time.

The optimization of the cost function requires the use of Euler-Lagrange Theorem. Consider the optimal control history,$u^*(t)$ and define $\eta(t)$ as a differentiable arbitrary function with a value of zero at the beginning and end of the time interval of interest. In order for $u^*(t)$ to minimize J the first order necessary condition given as

$$J[u^*] \leq J(u^* + \epsilon\eta) \tag{4.2}$$

must be true for an arbitrarily small ϵ[40]. Next a new function is defined with ϵ as the only input defined as

$$\Phi(\epsilon) = J(u * + \epsilon\eta) \tag{4.3}$$

By definition Equation (4.3) has a local minimum at $\epsilon = 0$. Thus the first order necessary condition must be true at that point. Notice that the necessary condition on the function $\Phi(\epsilon)$ is a function optimization problem rather than a functional optimization problem.Thus the necessary condition is reduced to a one dimensional derivative expressed as

$$\frac{d\Phi}{d\epsilon}|_{\epsilon=0} = \int \frac{dL}{d\epsilon}|_{\epsilon=0} dt = 0 \tag{4.4}$$

Taking the total derivative of the Lagrangian with respect to ϵ produces the relationship,

$$\frac{dL}{d\epsilon} = \frac{\partial L}{\partial u}\eta + \frac{\partial L}{\partial \dot{u}}\eta \tag{4.5}$$

Plugging Equation (4.5) back into Equation (4.4) results in

$$\int \frac{\partial L}{\partial u}\eta + \frac{\partial L}{\partial \dot{u}}\eta dt = 0 \tag{4.6}$$

Equation (4.6) is separated into two integrals and integration by parts is applied producing

$$\int \frac{\partial L}{\partial u}\eta dt + \frac{\partial L}{\partial \dot{u}}\eta| - \int \eta \frac{d}{dt}\frac{\partial L}{\partial \dot{u}} dt = 0 \tag{4.7}$$

Recall that η is defined as zero at the start and end of the interval of interest, therefore the 2nd term of Equation (4.7) is zero resulting in

$$\int \left(\frac{\partial L}{\partial u} - \frac{d}{dt} \frac{\partial L}{\partial \dot{u}} \right) \eta dt = 0 \tag{4.8}$$

In order to guarantee optimality, the equation must hold for any arbitrary function η. Therefore, the quantity in parenthesis must be zero at the optimal control. Setting this quantity to zero results in the Euler-Lagrange equation, expressed as

$$\frac{\partial L}{\partial u} - \frac{d}{dt} \frac{\partial L}{\partial \dot{u}} = 0 \tag{4.9}$$

also known as the necessary condition. Equation (4.9) must be true for the control, u^*, to produce a local minimum of the cost function. Additional derivations and discussion of E-L theorem are present in Lawden[21], Bryson and Ho[42], Longuski[26]

4.2 Hamiltonian

In addition to minimizing the cost function the control must meet constraints imposed by the equations of motion, $\bar{f}(\bar{x}, \bar{u}, t) = \dot{\bar{x}}$. In order to ensure the equations of motion are satisfied, they are adjoined to the Lagrangian to form a new functional known as the hamiltonian given as

$$H(\bar{x}, \bar{u}, \bar{\lambda}, t) = L(\bar{x}, \bar{u}, t) + \bar{\lambda}^T \bar{f}(\bar{x}, \bar{u}, t) \tag{4.10}$$

where $\bar{\lambda}$ is a vector of arbitrarily defined costates that are analogous to the use of lagrange multipliers in function optimization. For an n-dimensional system n costates are defined, each associated with a different state element. However, unlike lagrange multipliers the costates are functions of time rather than fixed variables.

In order to optimize the hamiltonian in Equation (4.10) the following two necessary conditions must be met. First the hamiltonian must be at a local extremum with respect to the control and secondly the Euler-Lagrange theorem as described in the previous subsection

must be true. The E-L theorem is rewritten for the optimization of the hamiltonian rather than the lagrangian resulting in the following necessary conditions.

1.

$$\frac{\partial H}{\partial u} = 0$$

2. From EL theorem

$$\frac{\partial H}{\partial x} - \frac{\partial}{\partial t}\frac{\partial H}{\partial \dot{x}} = 0$$

The first condition produces a relationship between the costates and the function $u(t)$, while the second condition gives a requirement on the time derivatives of the costates as

$$\frac{\partial H}{\partial x} = -\dot{\bar{\lambda}} \tag{4.11}$$

These conditions together result in a 2PBVP. Targeting methods as discussed in Chapter 3 are employed to solve the new formulation of the problem and produce optimal control histories.

An initial state and costate vector is propagated through the equations of motion to produce a trajectory through the system of interest. For this investigation the propagation occurs in the CR3BP+LT, but the method can be applied to any dynamic system. The costates at each point along the orbit inform the control function $u(t)$ in such a way that ensures the cost is minimized. For an autonomous system, such as the CR3BP+LT minimum energy and minimum fuel problems discussed further in Chapter 5, the hamiltonian is a constant throughout any optimal trajectory. This fact is demonstrated by calculating the total time derivative of th hamiltonian as

$$\frac{d}{dt}(H(\bar{x}, \bar{\lambda}, t)) = \frac{\partial H}{\partial \bar{x}}\dot{\bar{x}} + \frac{\partial H}{\partial \bar{\lambda}}\dot{\bar{\lambda}} + \frac{\partial H}{\partial t} \tag{4.12}$$

The partial derivative of H with respect to $\bar{x}$ is defined for an optimal arc by Equation (4.11). The partial derivative with respect to $\bar{\lambda}$ is the equations of motion $\bar{f}(\bar{x})$ by the definition of the hamiltonian. Therefore the total time derivative of the hamiltonian can be expressed as

$$\frac{d}{dt}(H(\bar{x},\bar{\lambda},t)) = -\dot{\bar{\lambda}}\dot{\bar{x}} + \dot{\bar{x}}\dot{\bar{\lambda}} + \frac{\partial H}{\partial t} \tag{4.13}$$

where the first two terms of Equation (4.13) cancel out to produce

$$\frac{d}{dt}(H(\bar{x},\bar{\lambda},t)) = \frac{\partial H}{\partial t} \tag{4.14}$$

The total time derivative of the hamiltonian along an optimal trajectory is its partial derivative with respect to time. Thus any system, where neither the Lagrangian nor the equations of motion are an explicit function of time, has a hamiltonian that remains constant throughout any optimally propagated trajectory.

4.3 Transversality

A transfer between two fixed states over a fixed Time Of Flight (TOF) results in a fully constrained 2PBVP. For an n dimensional system The free variables are the n costates and the constraint functions are the n target states. As represented below.

$$\bar{x} = \left[\bar{\lambda}_0\right], \bar{F} = \left[\bar{x}_f - Target\right] \tag{4.15}$$

However, additional degrees of freedom are often included in optimization problems especially for astrodynamic applications. Transfers may not contain a restriction on time of flight or initial and final states. These added freedoms require auxillary constraint functions to pose a well defined 2PBVP and select the new free variables optimally. The constraints are given by the transversality condition[42],

$$H_f dt_f - \bar{\lambda}_f^t d\bar{x}_f + H_0 dt_0 - \bar{\lambda}_0^t d\bar{x}_0 = 0 \tag{4.16}$$

where the subscripts 0 and f refer to the initial and final points on the optimal trajectory respectively. Equation (4.16) ensures that the added free variables are selected in such a way that minimizes the hamiltonian.

A derivation and further discussion of the transversality condition is available in Longuski[26]. The equation provides extra optimality constraints to select additional free variables optimally. For example if the TOF is allowed to vary then dt_f in Equation (4.16) becomes non-zero. As a result, the hamiltonian at the final time, H_f, must be zero to ensure the equation is satisfied. This reasoning is applied to all terms of the equation. Any additional freedom added to the problem results in a variation at the beginning or end of the trajectory having a non zero value. The transversality equation relates this variation to a new optimality condition thereby maintaining a square system.

5. OPTIMIZATION IN CISLUNAR TRANSFER DESIGN

In this chapter the methods of indirect optimization are discussed with applications to cislunar low thrust transfer design. The minimum fuel and minimum energy optimal low thrust transfer problems are formulated in the CR3BP. The cost functions of each problem are employed to construct their respective hamiltonians. Relationships between the costates and control are derived and a new STM is formulated for states and costates. The STM acts as a linear estimates of the final states and costates sensitivities with respect to the initial states and costates and these sensitivities are used to target optimal transfers. Additionally, the transversality condition optimally selects the location of departure and arrival for the transfer orbits.

The main challenge of the minimum fuel problem is its discontinuous thrust profile. This problem is addressed through a homotopy of sigmoid smoothing functions. As the homotopy parameter approaches zero the cost function approaches the minimum fuel cost and the thrust profile approximates a discontinuous function. The optimal transfer is then employed as an initial guess for a transfer that uses inertially fixed thrust vectors. The chapter concludes with a discussion of the targeting formulation for this inertially fixed transfer and its motivation.

5.1 Minimum Energy Problem

Fuel optimal transfers are often numerically difficult to compute due to the discontinuous nature of their thrust profiles discussed more in depth in section 5.2. In order to ease the process, a minimum energy transfer is computed to act as an initial guess for the minimum fuel solution. The cost function for this problem is stated as

$$J = \int \bar{u}(t)^2 dt \tag{5.1}$$

The equations of motion follow that of the CR3BP+LT dynamics as discussed in Chapter 2, with the control vector, $\bar{u}$, defining the three dimensional thrust vector of the low thrust engine. For this problem it is assumed that the control at any point in time is any element

of $\mathbb{R}^3$. The lack of constraint on the control magnitude allows the optimization process to result in a solution that requires thrust magnitude greater than the maximum achievable by contemporary propulsion technology. However, a good initial guess generally results in attainable thrust magnitudes. Additionally, the minimum energy problem is merely employed as an initial guess for the minimum fuel strategy. It is not necessary for it to meet any operational constraints. The minimum fuel formulation implements an implicit path constraint on thrust magnitude to ensure a implementable thrust profile. This technique is discussed more in later sections of this chapter.

A hamiltonian is constructed by adjoining the lagrangian to the equations of motion to form

$$H = \bar{u}^2 + \lambda_x \dot{x} + \lambda_y \dot{y} + \lambda_z \dot{z} + \lambda_{\dot{x}} f_x + \lambda_{\dot{y}} f_y + \lambda_{\dot{z}} f_z \tag{5.2}$$

Where the subscripts on the equations of motion, f, indicate the coordinate of the particular equation, while subscripts of the costates, λ, indicate the state element that is associated with the particular costate. The hamiltonian is not an explicit function of time and therefore is constant for this problem.

It is convenient at times to refer to subsections of the costate vector such as the costates associated with position or velocity state elements. These subvectors are denoted as λ_r and λ_v respectively. By Euler-Lagrange theorem the thrust control is related to the costates by

$$\bar{u} = -\frac{1}{2}\bar{\lambda}_v \tag{5.3}$$

The steering law restriction presented in Equation (5.3) is consistent with Lawden's primer vector. Lawden's Primer Vector theory forces tangency between the control input and the velocity costates in order for the minimum principle to be upheld[21].

The E-L theorem also gives the optimal derivatives of the costates from Equation (4.11). These derivatives are integrated to form the control history throughout the transfer. The differential equations for the costates are

$$\dot{\bar{\lambda}}_r = -\begin{bmatrix} U^*_{xx} & U^*_{xy} & U^*_{xz} \\ U^*_{xy} & U^*_{yy} & U^*_{yz} \\ U^*_{xz} & U^*_{yz} & U^*_{zz} \end{bmatrix} \bar{\lambda}_v \tag{5.4}$$

$$\dot{\bar{\lambda}}_v = -\bar{\lambda}_r + 2\begin{bmatrix} \lambda_{\dot{y}} \\ \lambda_{\dot{x}} \\ 0 \end{bmatrix} \tag{5.5}$$

Optimal trajectories are expressed by the CR3BP+LT equations of motion along with the equations of motion for the six associated costates in Equations (5.4) and (5.5). This reformulation of the optimization problem increase the number of differential equations to a twelve dimensional system. However, 2PBVPs in this system are generally smooth and have relatively large solution basins compared to formulations of the minimum fuel problem. As a result, the minimum energy transfer problem is solved first and acts as an initial guess for the minimum fuel problem.

5.1.1 Transversality of Orbit to Orbit Transfers

Cislunar orbit transfer applications generally involve a transfer between specific orbits rather than specific states. The orbit that the transfer originates is known as the source, while the destination orbit is called the sink. The phasing along the orbits is free to change and this added freedom may allow for greater cost reduction. The transversality condition is employed to select the points on the orbits that the transfer intersects. A diagram in Figure 5.1 highlights the freedoms in the orbit to orbit problem. The values of τ_1 and τ_2 represent the time along the source and sink orbits where the thrusting begins and ends. The transversality condition is implemented to select these times optimally resulting in cheaper transfers than the fixed state problem.

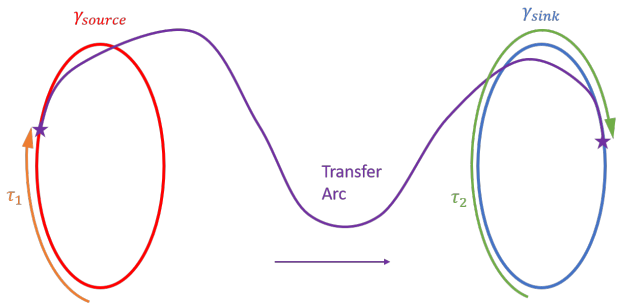

Figure 5.1. Orbit to orbit optimal transfer problem

The transversality condition is implemented to ensure the optimality of the initial and final state. In this investigation time of flight remains fixed to avoid successive iterations of the targeting process moving toward the globally optimal infinite time solution thereby preventing convergence[24]. The fixed TOF implies the initial and final times of the transfer cannot vary, therefore dt_f and dt_0 are zero. As a result, the transversality condition does not place a constraint on the value of the hamiltonian. The initial and final states are not fixed however. Each state has one degree of freedom in the form of time along the orbits. Therefore, these variations are written in terms of τ as

$$d\bar{x}_0 = \dot{\bar{x}}_0 d\tau_1 \tag{5.6}$$

$$d\bar{x}_f = \dot{\bar{x}}_f d\tau_2 \tag{5.7}$$

Equations (5.6) and (5.7) are plugged into Equation (4.16) to create two new optimality constraints for τ_1 and τ_2 thereby creating a square system. The final transversality constraints are listed as

$$\bar{\lambda}_0 \cdot \dot{\bar{x}}_0 = 0 \tag{5.8}$$

$$\bar{\lambda}_f \cdot \dot{\bar{x}}_f = 0 \tag{5.9}$$

and final targeting problem is now defined by the free variables and constraints,

$$\bar{x} = \begin{bmatrix} \bar{\lambda}_0 \\ \tau_1 \\ \tau_2 \end{bmatrix}, \bar{F} = \begin{bmatrix} \bar{x}_f - \gamma_{sink}(\tau_2) \\ \bar{\lambda}_0 \cdot \dot{\bar{x}}_0 \\ \dot{\lambda}_f \cdot \dot{\bar{x}}_f \end{bmatrix} \tag{5.10}$$

The targeting problem for the minimum energy transfers between orbits is fully constrained with 8 free variables and 8 constraints. Due to the numerical challenges in targeting these transfers a mutliple shooting scheme is employed to solve the problem. Constraint derivatives are computed using an STM of the same form as the STM in Chapter 3 however with additional entries for the costate vector.

5.1.2 Minimum Energy STM

A newton-rhapson targeting method is applied to solve the 2 point boundary value problem and compute a minimum energy transfer. The partial derivative of each constraint with respect to each variable is required to form the jacobian of the update equation given in Equation (3.16). In the jacobian matrix the effects of changing the initial states or costates on the final states and costates is linearly estimated using an STM similar to the state only STM discussed in Chapter 3. The STM for the minimum energy problem is a 12 by 12 matrix with an initial value equal to identity. As with the ballistic STM, its derivative is calculated at each time step and integrated with the trajectory. The linearization is given as

$$A_{minE} = \begin{bmatrix} A_{bal} & \frac{\delta \bar{x}_f}{\delta \bar{\lambda}_0} \\ \frac{\delta \bar{\lambda}_f}{\delta \bar{x}_0} & \frac{\delta \bar{\lambda}_f}{\delta \bar{\lambda}_0} \end{bmatrix} \tag{5.11}$$

$$\frac{\delta \bar{x}_f}{\delta \bar{\lambda}_0} = \begin{bmatrix} 0_3 & 0_3 \\ 0_3 & -\frac{1}{2} I_3 \end{bmatrix} \tag{5.12}$$

$$\frac{\delta \bar{\lambda}_f}{\delta \bar{\lambda}_0} = \begin{bmatrix} 0_3 & -U_2^* \\ -I_3 & \Omega \end{bmatrix} \tag{5.13}$$

$$\frac{\delta\bar{\lambda}_f}{\delta\bar{x}_0} = \begin{bmatrix} G_1 & G_2 & G_3 \\ G_2 & G_4 & G_5 \\ G_3 & G_5 & G_6 \end{bmatrix} \tag{5.14}$$

Where the G entries consist of 3rd derivatives of the pseudo-potential. The subscript 2 under U^* in Equation (5.13) refers to the fact that these entries are the matrix of all second derivatives of U^* as written in Equation (5.4). The equations for each value of G is

$$G_1 = -\lambda_v \cdot \begin{bmatrix} U^*_{xxx} \\ U^*_{xxy} \\ U^*_{xxz} \end{bmatrix} \tag{5.15}$$

$$G_2 = -\lambda_v \cdot \begin{bmatrix} U^*_{xxy} \\ U^*_{xyy} \\ U^*_{xyz} \end{bmatrix} \tag{5.16}$$

$$G_3 = -\lambda_v \cdot \begin{bmatrix} U^*_{xxz} \\ U^*_{xyz} \\ U^*_{xzz} \end{bmatrix} \tag{5.17}$$

$$G_4 = -\lambda_v \cdot \begin{bmatrix} U^*_{xyy} \\ U^*_{yyy} \\ U^*_{yyz} \end{bmatrix} \tag{5.18}$$

$$G_5 = -\lambda_v \cdot \begin{bmatrix} U^*_{xyz} \\ U^*_{yyz} \\ U^*_{yzz} \end{bmatrix} \tag{5.19}$$

$$G_6 = -\lambda_v \cdot \begin{bmatrix} U^*_{xzz} \\ U^*_{yzz} \\ U^*_{zzz} \end{bmatrix} \tag{5.20}$$

These matrices are integrated along with the equations of motion to produce an STM for both the states and costates. The matrix at the end of th propagation relates changes in the initial state and costate elements with changes in the final state and costate elements.

The minimum energy problem has solutions that continuously vary thrust direction and magnitude. These long term continuous maneuvers are not possible for actual spacecraft to implement. Additionally, the optimal minimum fuel transfers use less propellant than the minimum energy transfers by definition. The minimum fuel problem is solved using a multiple shooting newton-rhapson targeting scheme, similar to the minimum energy solution. However, this problem results in limited duration, fixed thrust magnitude maneuvers that adhere more closely to modern spacecraft capabilities. The value of initially solving the minimum energy problem is that its continuous nature makes it more numerically stable and less sensitive than the minimum fuel problem. The resulting solution of the minimum energy problem is used as an initial guess to improve the convergence of the minimum fuel problem.

5.2 Minimum Fuel Problem

Ultimately the minimum fuel solution is preferred to the minimum energy solution due to its lower propellant cost and implicit constraint on the thrust magnitude. This problem has a cost function of

$$J = \int |u(t)| dt \tag{5.21}$$

The same analysis as described in section 5.1 is employed to construct the hamiltonian as well as the optimal time derivatives for the costates. The hamiltonian of this cost function is constructed as

$$H = |\bar{u}| + \lambda_x \dot{x} + \lambda_y \dot{y} + \lambda_z \dot{z} + \lambda_{\dot{x}} f_x + \lambda_{\dot{y}} f_y + \lambda_{\dot{z}} f_z \tag{5.22}$$

The derivative of Equation (5.22) with respect to the control is computed to produce the optimal thrust vector given by

$$\lambda_v = -\frac{\bar{u}}{|u|} \tag{5.23}$$

While the construction of this necessary condition is the same for all indirect optimization problems, the relation between the optimal control vector and the costates has new features in this formulation that must be explicitly addressed.

Notice in Equation (5.23) the control vector is not fully determined. The thrust must point in the opposite direction of the pointing vector, but the primer vector only gives information about the thrust unit vector the thrust magnitude is not explicitly stated. According to Pontriagin's principle the minimum fuel solution is achieved through a bang-coast-bang thrust profile[40]. This refers to a spacecraft thrusting at a maximum value for sections of the transfer while coasting during others. A switching function is implemented to determine when thrusting or coasting is optimal. The switching function for a fixed mass spacecraft is given as

$$S = |\lambda_v| - 1 \tag{5.24}$$

When S is negative the spacecraft coasts and when S is positive the spacecraft must thrust at a maximum thrust magnitude for an optimal trajectory. Therefore, the minimum fuel problem requires a predefined maximum thrust magnitude for the solution to exist. The advantage of this finding is that there is no risk of the optimal solution computed by the targeting process requiring an overly large thrust magnitude at any point along the transfer. However, a drawback is that the thrust profile is discontinuous. Discontinuities in the differential equations cause targeting methods, such as the newton-rhapson method implemented in this investigation, to struggle. Section 5.3 discusses how this problem is addressed through the use of sigmoid smoothing functions.

5.3 Sigmoid Smoothing

Sigmoid smoothing, also known as a logarithmic penalty function, is used to ease the numerical challenges with taregting fuel optimal low thrust transfers. This method uses a sigmoid function to smoothly approximate the discontinuous nature of the fuel optimal control history. A homotopy variable, ϵ, is employed to transition the solution from a smooth, easily integrable function to a nearly discontinuous optimal fuel trajectory. There are several methods for smoothly transitioning to the optimal thrust trajectory including a

linear combination of minimum fuel and minimum energy[43], a homotopy in the exponent of the lagrangian[44], or the sigmoid smoothing function[45], [46]. Parrish implements these methods on a variety of transfer scenarios and concludes that the sigmoid function converges most reliably and with the fewest number of homotopy steps. The advantage of the sigmoid function is that it ensures the control vector is a differentiable function of the costates at all control magnitudes. The linear homotopy is discontinuous at both the minimum and maximum thrust values, while the exponent homotopy is discontinuous at only the maximum thrust values[25]. Sigmoid smoothing is implemented in this investigation due to the fully continuous nature of the produced control resulting in better numerical accuracy of the STM approximations. The cost function for the sigmoid smoothed optimal fuel trajectory is

$$J = \int |\bar{u}| + \epsilon[\bar{u} ln \bar{u} + (1 - \bar{u}) ln(1 - \bar{u})]dt \tag{5.25}$$

Notice that for small values of ϵ the cost function approaches the minimum fuel problem cost, Equation (5.21). The new optimal magnitude and direction of the control vector are again calculated using E-L theory. The control vector must follow Lawden's pointing vector, but as opposed to the unsmoothed minimum fuel problem a continuous function defines the magnitude of th vector. The optimal direction and magnitude are

$$|u| = -\frac{T_{max}}{2}[1 + tanh\left(\frac{S}{2\epsilon}\right)] \tag{5.26}$$

and

$$\hat{u} = -\hat{\lambda}_v \tag{5.27}$$

respectively. In Equation (5.26), T_{max} is the maximum thrust acceleration that the spacecraft can produce. As ϵ approaches zero the thrust magnitude approximates a step function between 0 and the maximum thrust magnitude. In order to find solutions with ϵ near zero first solutions are computed for large values of ϵ. The solutions then act as an initial guess for a reduced ϵ value. This process is continued until the thrust profile of the solution well approximates a step function. This iterative solving of similar problems with a successively changing parameter is known as homotopy. Beginning with a smooth easily differentiable

control law ensures convergence due to the wider attraction basin of solutions in the less sensitive problem. The produced solution is then likely within the smaller basin of attraction for the subsequent slightly more sensitive problem, provided the homotopy parameter is reduced slowly. A figure of the homotopy process is given in Figure 5.2. Figure 5.2 exhibits

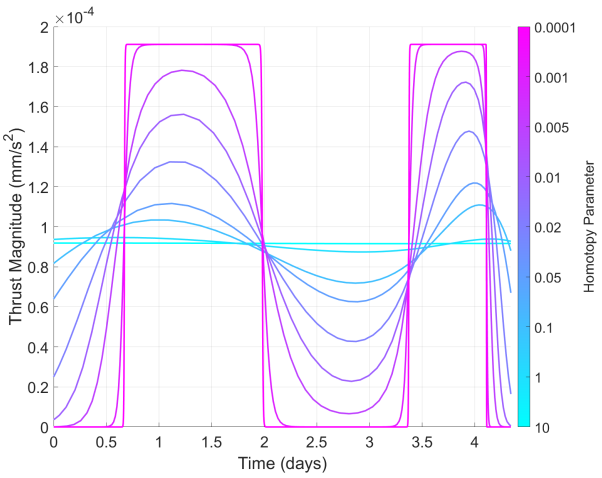

Figure 5.2. Evolution of an arbitrary low thrust arc as epsilon decreases

the thrust profile for an arbitrary transfer between two states in the CR3BP with a variety of ϵ values. The larger ϵ solutions have smooth thrusting throughout the entire transfer. The smallest ϵ appears almost completely discontinuous with jumps between zero and the maximum thrust magnitude.

One challenge when implementing the sigmoid smoothing technique is selecting the initial value for ϵ. Small values are challenging to converge but overly large values also have numerical limitations. The computation of STM elements for large ϵ require the subtraction of large similar valued numbers. Thus the STM for these problems acts as a poor approximation for the costate sensitivities. A lack of accurate constraint derivatives causes the newton-rhapson targeting scheme to struggle. Generally, well-behaved convergence properties are achieved for cislunar transfer applications by setting the initial ϵ to a value of 1.

5.4 Inertially Fixed Thrust Solutions

The fuel optimal solutions have a bang-coast-bang geometry in thrust magnitude, but the thrust direction still varies continuously during thrusting arcs. This geometry requires constant gimbaling of thrusters and precise attitude control for an actual spacecraft to follow the flight path. This requirement makes the solutions practically infeasible. After constructing the fuel optimal transfers a final targeting problem is employed to produce a solution that has a thrust vector fixed in the inertial frame. The Inertially Fixed Thrust Transfer (IFTT) is the last solution computed throughout this design process. Other practical constraints can be added during this design step such as a maximum thrust time per arc, direction restriction to allow favorable spacecraft orientation, or specific duty cycle restrictions.

The solution to the minimum fuel problem acts as an initial guess where each thrust arc is set to an inertially fixed direction and the coast arcs are unchanged. The inertially fixed thrust direction is initially set to the thrust direction at the beginning of the thrust arc in the minimum fuel solution. Simply using the initial thrust vector is sufficient for convergence of the applications posed in this investigation, however using an average vector over the arc as discussed by Lafarge may form a closer initial guess for more sensitive problems[47]. The new targeting problem is similar to those previously discussed however the thrust components are directly selected by the targeter rather than a function of costates. The problem formulation is

$$\bar{X} = \begin{bmatrix} \bar{x}_2 \\ \vdots \\ \bar{x}_{n-1} \\ \bar{T}_1 \\ \vdots \\ \bar{T}_m \\ \tau_1 \\ \vdots \\ \tau_n \end{bmatrix}, \bar{F} = \begin{bmatrix} \bar{x}_2 - \bar{x}_3 \\ \vdots \\ \bar{x}_{n-1} - \bar{x}_n \\ |\bar{T}_1| - T_{max} \\ \vdots \\ |\bar{T}_m| - T_{max} \end{bmatrix} \tag{5.28}$$

In Equation (5.28) there are n total arcs along the transfer m of which are thrusting arcs. The inertially fixed thrust direction for the ith arc is denoted $\bar{T}_{\mathrm{i}}$, and τ_{i} is propagation time for each arc. The maximum thrust for the specific spacecraft, T_{max}, is set to a value that matches the spacecraft capabilities. The IFTT targeter produces extremely cheap transfers because the initial guess is optimal, however no optimality constraint is included in this targeting scheme. The thrust is treated as a parameter of the equations of motion for each thrusting arc and therefore the method for determining the derivatives of state with respect to a parameter is employed as discussed in section 3.3. A diagram of a optimal fuel thrusting arc and associated IFTT solution is depicted in Figure 5.3.

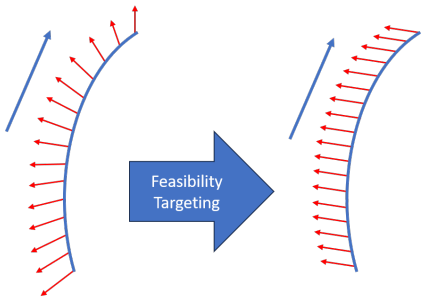

Figure 5.3. Initial optimal thrust arc compared to fixed thrust direction arc

The diagram depicts thrust arcs in th inertial frame. Both arcs hav a constant thrust magnitude however before IFTT targeting the thrust vectors continuously change direction as opposed to after the IFTT targeting where the direction is fixed. While optimality is lost in this step of the transfer design process the final transfers require very little propellant. For the example transfers produced in this investigation all IFTTs remain close in propellant cost to the minimum fuel transfers and most require less propellant than the minimum energy solutions.

The methods discussed in this chapter allow for rapid propellant efficient transfer design within cislunar space. The method leverages, the large basin of attraction for solutions in the minimum energy problem, the propellant savings of the minimum fuel solution, and the numerical stability of sigmoid smoothing. Through these intermediate problems a propellant efficient initial guess is produced for use in the IFTT targeter. Overall, these methods mitigate the challenges with indirect optimization for low thrust transfer design applications.

The strengths of the minimum fuel and minimum energy problem formulations work in tangent to inform the IFTT design.

6. RESULTS

The main challenge in producing optimal transfers with indirect optimization is in selecting the initial values for the costates. In general the costates do not have physical meaning thus intuition about what makes a good initial guess is hard to develope. Authors have analyzed multiple methods for determining these values including direct optimization, neural nets, adjoint control laws, etc.[25], [45], [46], [48].These methods have varying levels of success but are generally computationally expensive. However, setting all costates to zero does have physical interpretation. A ballistic structure allows DST to produce insights into the natural dynamics of the system. These insights are leveraged during the transfer construction process.

In this chapter the transfer design techniques discussed in chapter 5 are applied to a variety of sample missions between multi-body orbits. The transfers are grouped into three categories based on the ballistic structures used as an initial guess for the targeting process. The first category includes transfers that leverage multi-body orbits for an initial guess. These transfers connect orbits of the same family. Orbit families in the CR3BP are continuous. As a result, for any two orbits in the same family there must exist orbits between them with similar characteristics. Segments of the intermediate orbits are leveraged to seed the targeting problem with ballistic trajectories. For transfers between orbits of different families, the stable and unstable manifolds act as an initial guess. This formulation takes advantage of the natural flow to and away from unstable orbits in the CR3BP. Additionally, manifolds tend to traverse large regions of cislunar space and therefore provide many opportunities for transit. The final category consists of transfers that require stretching directions for initial guess construction. This method is necessary to produce transfers between stable orbits of different families.

The system parameters for this investigation are located in Table 6.1 and the spacecraft specific parameters are located in Table 6.2. The spacecraft mass, specific impulse, and max thrust force are based on the Deep Space 1 mission[9] with max thrust acceleration computed from force and mass. The parameters are the same for all the presented example transfer problems but the specific values are not required for the design process. The techniques

discussed in this investigation are generalizable to any spacecraft by changing the spacecraft parameters. Additionally, throughout this chapter the computed low thrust transfers are

Table 6.1. System parameters for transfer generation

Parameter	Value	Units
Mass Ratio (μ)	0.01215361	ND
Characteristic Length (l^*)	384400	Km
Characteristic time (t^*)	3.751951907852177e5	sec

Table 6.2. Spacecraft parameters for transfer generation

Parameter	Value	Units
Spacecraft Mass (m_3)	500	kg
Max Thrust Force (F_T)	92	mN
Max Thrust Acceleration (T)	0.1841	mm/s^2
Specific Impulse (I_{sp})	2200	s

compared to the TMVD between the orbits or an impulsive transfer from the literature. These ΔV values are converted to propellant mass based on Equation (2.43). For comparison the impulsive spacecraft is assumed to be the same mass as the low thrust spacecraft (500 kg), with infinite max thrust force and a specific impulse of 400s.

6.1 Leveraging Intermediate Orbits

The transfers produced in this section move between orbits in the same family by leveraging intermediate family members as initial guesses. This initial guess formulation is highly effective for same family transfers because of the continuous nature of orbit families in autonomous systems. Any two orbits within a family are guaranteed to have an additional orbit between them. The first transfer discussed moves from an L_1 northern halo orbit with a Jacobi Constant of 3.16 to an L_1 northern halo with a Jacobi Constant of 3.11. Additional characteristics of the orbits as well as there initial conditions are given in Table 6.3.

The first step in the transfer construction process is to select segments of intermediate orbits to act as an initial guess for the targeting process. The segments are selected as half

Table 6.3. Characteristics of L_1 halo orbits used in transfer

Parameter	Source Orbit	Sink Orbit
Family	L_1 Northern Halos	L_1 Northern Halos
Jacobi Constant	3.16	3.11
Period (days)	11.9598	12.0883
z-Amplitude (km)	16,032	36,236
Stability Index ($\|\bar{\lambda}\|_\infty$)	1,835	682
Initial Position (ND)	[0.8630,0,-0.0351]	[0.8919,0,-0.0697]
Initial Velocity (ND)	[0,-0.1673,0]	[0,-0.2633,0]

of each intermediate orbit and are evenly spaced in Jacobi Constant. Using half orbits as the initial guess is somewhat arbitrary, but later transfers in this section discuss the implications of changing the initial guess formulation. The Initial guess for this example is depicted in Figure 6.1.

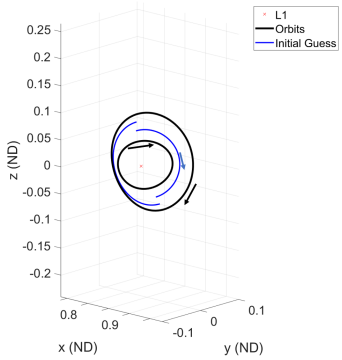

Figure 6.1. Initial guess for a low thrust transfer between halo orbits, leveraging intermediate orbits

The corrections process as discussed in Chapter 3 is performed to produce an energy optimal solution between these two orbits. This transfer given in Figure 6.2. Has a time of flight of 24.09 days and uses 3.4685 kg of fuel. The thrust profile is presented in figure Figure 6.3 The resulting propellant mass cost is compared to the TMDV between the two orbits. As discussed in Chapter 3 the TMDV depends on the location the maneuver takes place. The TMDV for the same family transfers is computed as the smallest TMDV for a single maneuver at any point on either of the two orbits. While it is unlikely that for

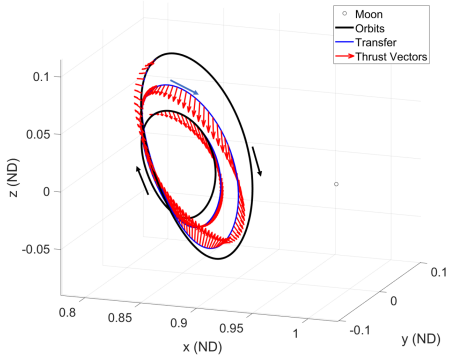

Figure 6.2. Minimum energy transfer between L_1 northern halo orbits from JC = 3.16 to JC = 3.11

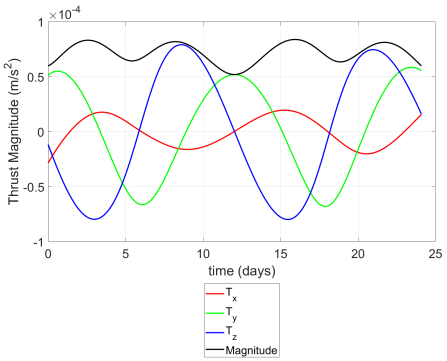

Figure 6.3. Minimum energy thrust profile between L_1 northern halo orbits from JC = 3.16 to JC = 3.11

these orbits a transfer exists that follows all the assumptions of the TMDV, it provides a metric to compare to the low thrust transfer. For these orbits the TMDV is 112 m/s, therefore 14.4748 kg of propellant is required for an impulsive transfer between these orbits. The added efficiency of the high I_{sp} low thrust engine produces a transfer with over 75% reduction in propellant cost.

More propellant savings can be produced by solving the minimum fuel problem. The minimum energy solution is used as an initial guess to ensure convergence of this slightly more sensitive transfer. As discussed in Chapter 5 sigmoid smoothing is employed to approximate the optimal bang-coast-bang solution. The resultant transfer along with its thrust profile is given in Figures 6.4 and 6.5. The new time of flight and fuel mass are 24.09 days and

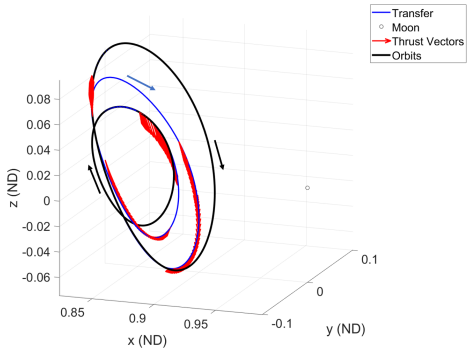

Figure 6.4. Minimum fuel transfer between L_1 northern halo orbits from JC = 3.16 to JC = 3.11

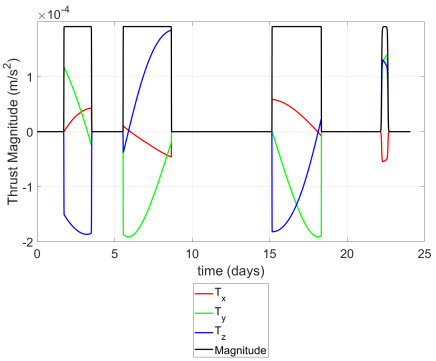

Figure 6.5. Minimum fuel thrust profile between L_1 northern halo orbits from JC = 3.16 to JC = 3.11

3.2524 kg respectively. Notice the TOF is unchanged due to the fixed time constraint. As previously discussed in Chapter 5, the fixed time constraint prevents the movement of the solution toward the infinite time global optimal. As expected, the minimum fuel has lower propellant consumption than the minimum energy solution, however the savings are small. An additional benefit of implementing the minimum fuel transfer is that there is an implicit constraint placed on the magnitude of the thrust vector. This constraint ensures that the thrust is not greater than the capabilities of the spacecraft or too small for implementation as visible in Figure 6.5. Notice that the black curve in the figure representing the thrust magnitude acts as a good approximation of a step function. However, the x, y, and z components of the control vary smoothly while thrusting. The continuous reorientation of

the thrust vector is not practical for real spacecraft, therefore the IFTT targeter must be implemented to find the final transfer.

The continuously changing thrust directions must be fixed in the inertial frame to meet operational constraints. A final targeting problem produces an IFTT that no longer maintains optimality, but is near the optimal solution and therefore very low cost. The resulting transfer and thrust profile are in Figures 6.6 and 6.7. The transfer requires 3.7934 kg of propellant and has a TOF of 22.5150 days. Notice the fuel consumption has slightly increased due to the loss of optimality but it is still more efficient than the impulsive TMDV due to the added efficiency of the low thrust engine and the low cost of the initial guess. Additionally, the thrust profile is fixed in the inertial frame. The thrust vector $\bar{T}^I = [T_x^I, T_y^I, T_z^I]$ is plotted for this solution rather than the thrust vector in rotating frame coordinates. Therefore, the thrust components do not change with time as visible in Figure 6.7. Lastly, the TOF is 1.5 days shorter than the optimal transfers. TOF is allowed to vary in this targeting problem freely thus the shorter time of flight is not guaranteed by the IFTT targeter. In general the IFTT TOF may be longer, shorter, or roughly the same length as the optimal transfers depending on the exact application. Table 6.4 summarizes the time of flight and propellant

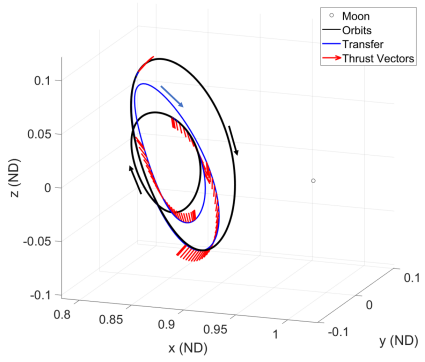

Figure 6.6. IFTT between L_1 northern halo orbits from JC = 3.16 to JC = 3.11

mass consumption for each converged transfer, as well as the propellant cost for the TMDV using an impulsive engine.

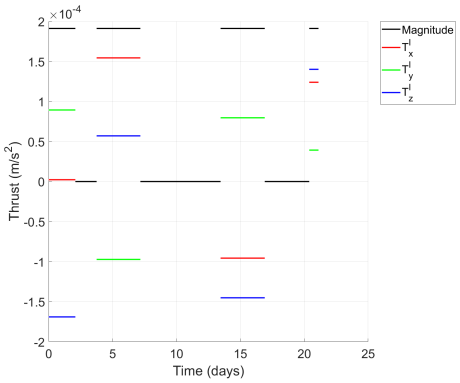

Figure 6.7. IFTT thrust profile between L_1 northern halo orbits from JC = 3.16 to JC = 3.11

Table 6.4. Summary of L_1 halo orbit transfers

Transfer	Fuel Mass (kg)	Time of Flight (days)
Minimum Energy	3.4685	24.0902
Minimum Fuel	3.2524	24.0902
IFTT	3.7934	22.5150
Impulsive TMDV	14.4748	n/a

6.1.1 Additional Revolutions

The same transfer is computed again using more intermediate orbit segments for the initial guess. Because the indirect optimization process produces a local minimum in the cost function, experimentation with the initial guess results in different locally optimal transfers. These other optimal solutions may be of interest depending on the application. For the L_1 halo orbit example, additional intermediate segments act as the initial guess to produce a longer time of flight transfer with lower propellant cost. This initial guess is shown in figure Figure 6.8. The resultant minimum energy, minimum fuel and IFTT transfers along with their thrust profiles are given in Figures 6.9 to 6.14. Additionally, Table 6.5 summarizes propellant cost and times of flight of the converged transfers.

The most notable difference between these transfers and the original set of transfers between the same orbits is their time of flights. The construction process leveraged twice as many intermediate orbit segments resulting in transfers with approximately double the

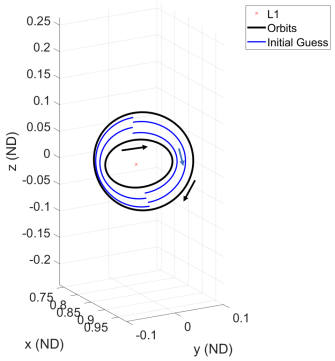

Figure 6.8. Initial guess using additional revolutions to transfer between L_1 northern halos at JC = 3.16 and 3.11

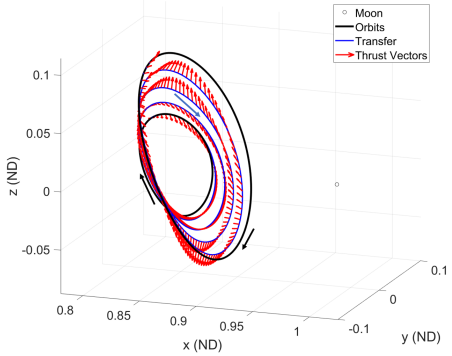

Figure 6.9. Minimum energy transfer between L_1 northern halos at JC = 3.16 and 3.11 leveraging additional revolutions

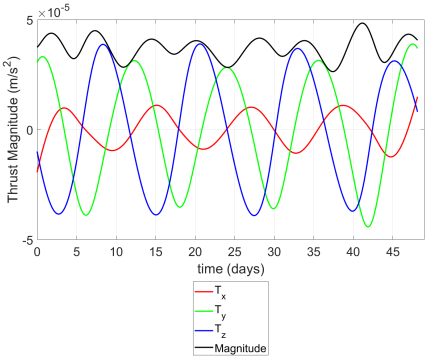

Figure 6.10. Thrust profile of the minimum energy transfer between L_1 northern halos at JC = 3.16 and 3.11 leveraging additional revolutions

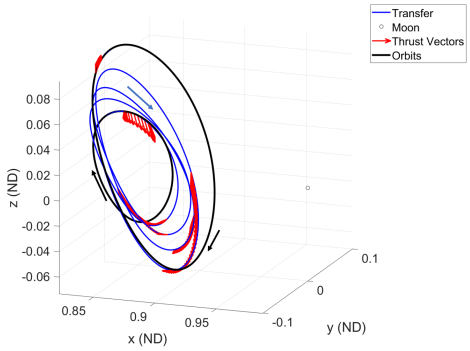

Figure 6.11. Minimum fuel transfer between L_1 northern halos at JC = 3.16 and 3.11 leveraging additional revolutions

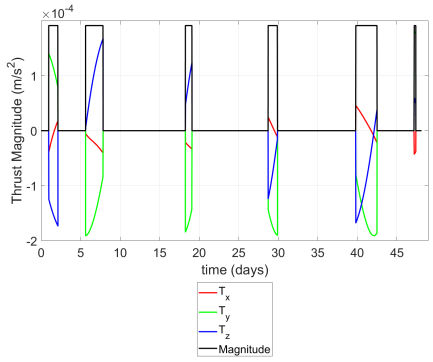

Figure 6.12. Thrust profile of the minimum fuel transfer between L_1 northern halos at JC = 3.16 and 3.11 leveraging additional revolutions

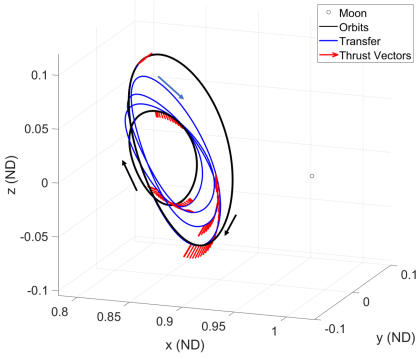

Figure 6.13. IFTT between L_1 northern halos at JC = 3.16 and 3.11 leveraging additional revolutions

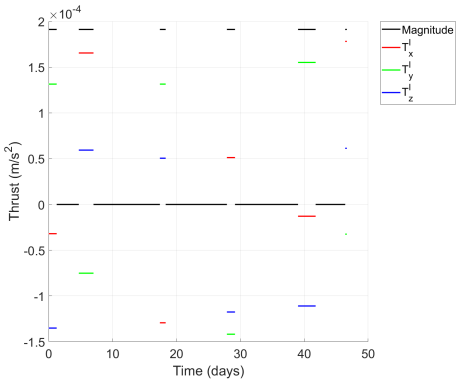

Figure 6.14. Thrust profile of the IFTT between L_1 northern halos at JC = 3.16 and 3.11 leveraging additional revolutions

Table 6.5. Summary of L_1 halo orbit transfers with longer times of flight

Transfer	Fuel Mass (kg)	Time of Flight (days)
Minimum Energy	3.5774	48.1228
Minimum Fuel	3.1760	48.1228
IFTT	3.3791	47.3931
Impulsive TMDV	14.4748	n/a

time of flight. However, an advantage of the longer time of flight is that the minimum fuel and IFTT transfers use less propellant than their shorter counterparts. While the propellant savings are relatively small, some spacecraft may elect to follow longer time of flight transfers for applications where propellant mass is a limiting constraint. The minimum energy transfer does not have lower propellant cost, however, the thrust magnitude of the transfer is reduced, as evident by comparing Figures 6.3 and 6.10. This lower magnitude could be useful when transitioning to minimum fuel transfers with lower maximum thrust capabilities.

6.1.2 Northern to Southern Halos

The process of computing solutions for increasingly challenging problems is repeated for a transfer between an L_1 northern halo and an L_1 southern Halo with JC = 3.1694. The orbit characteristics are summarized in Table 6.6. These orbits are selected because a heteroclinic transfer exists between them. The free transfer between these orbits is computed by Haapala [20]. Figure 6.15 is a copy of the figure illustrating the geometry of the free transfer. By

definition the heteroclinic represents a propellant free transfer between these two orbits. It leverages the manifolds to asymptotically depart and approach the orbits. As a result, it is not possible for the low thrust transfer to use less propellant, however the heteroclinic has a relatively long time of flight of 74.7445 days. In this case the advantage of the low thrust transfer is that the TOF can be greatly reduced for a small increase in propellant cost.

Table 6.6. Characteristics of L_1 halo orbits with a heteroclinic connections

Parameter	Source Orbit	Sink Orbit
Family	L_1 northern halo	L_1 southern halo
Jacobi Constant	3.1694	3.1694
Period (days)	11.9285	11.9285
z-Amplitude (km)	9,308	9,308
Stability Index ($\|\bar{\lambda}\|_\infty$)	2167	2167
Initial Position (ND)	[0.8577,0,-0.0208]	[0.8577,0,0.0208]
Initial Velocity (ND)	[0,-0.1459,0]	[0,-0.1459,0]

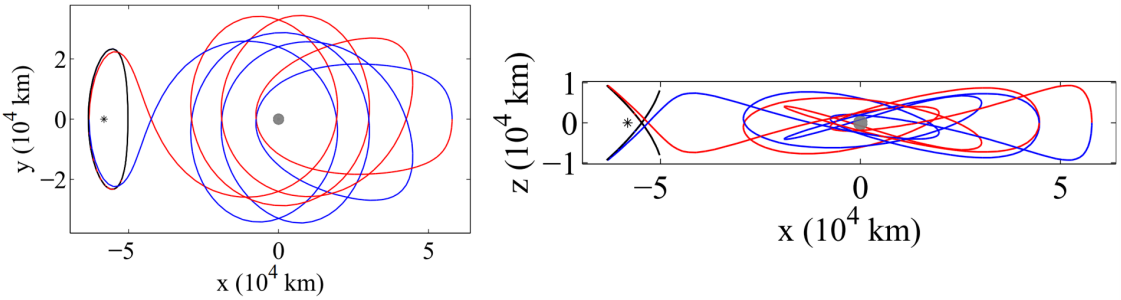

Figure 6.15. Reproduction of Haapala's heteroclinic transfer between L_1 northern halo and L_1 southern halo at JC = 3.1694

The northern and southern sections of the L_1 halo orbits are subsections of the same family. Thus there exists a continuous set of orbits containing both the northern and southern halos. The construction of free transfers between these orbits requires the orbits stable and unstable manifolds, however the construction of low thrust transfers can leverage the intermediate orbits within the family. The initial guess for the optimization problem is constructed using segments of these orbits. The initial guess is depicted in Figure 6.16. The minimum energy, minimum fuel, and IFTT transfers along with their thrust profiles are shown in Figures 6.17 to 6.22. They are constructed following the same methodology

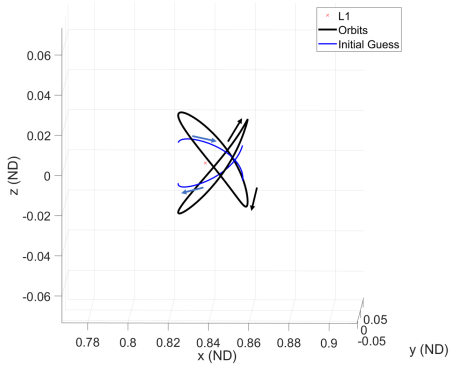

Figure 6.16. Initial Guess for a transfer between L_1 northern and southern halo orbits at JC = 3.1694

as employed for the previous transfer problems in this section. Table 6.5 summarizes these solutions.

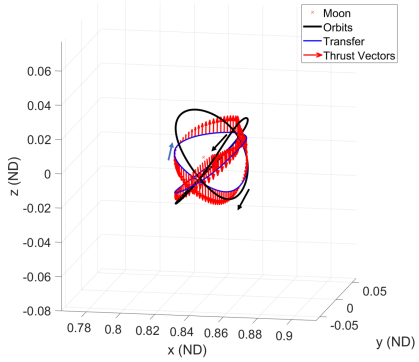

Figure 6.17. Minimum energy transfer between L_1 northern and southern halo orbits at JC = 3.1694

Table 6.7. Summary of transfers between L_1 northern and southern halo orbits

Transfer	Fuel Mass (kg)	Time of Flight (days)
Minimum Energy	3.0906	23.7956
Minimum Fuel	2.4950	23.7956
IFTT	2.4939	23.8354
heteroclinic	0	74.7445

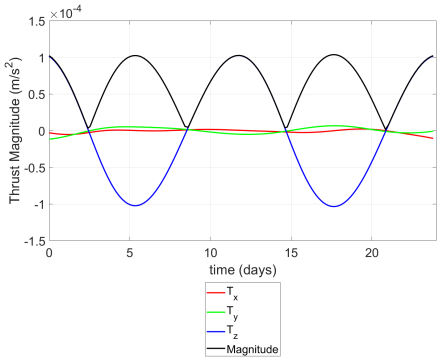

Figure 6.18. Thrust profile of a minimum energy transfer between L_1 northern and southern halo orbits at JC = 3.1694

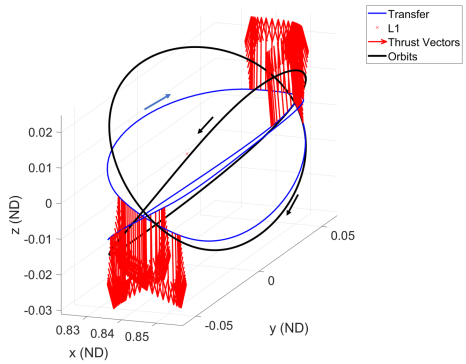

Figure 6.19. Minimum fuel transfer between L_1 northern and southern halo orbits at JC = 3.1694

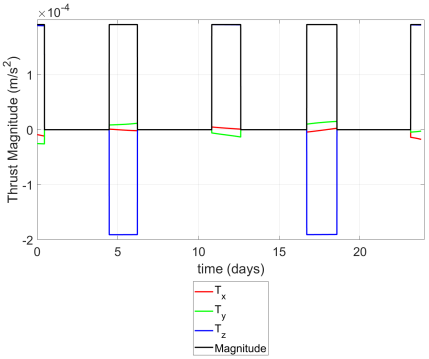

Figure 6.20. Thrust profile of minimum fuel transfer between L_1 northern and southern halo orbits at JC = 3.1694

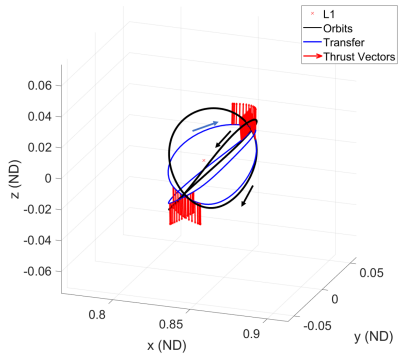

Figure 6.21. IFTT between L_1 northern and southern halo orbits at JC = 3.1694

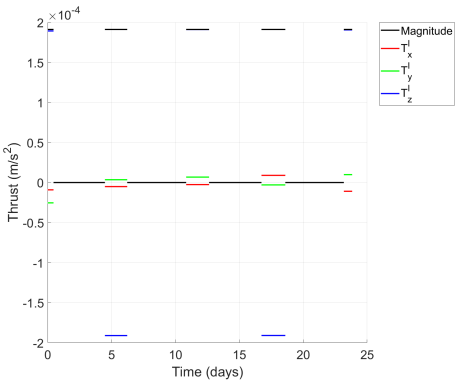

Figure 6.22. Thrust profile of IFTT between L_1 northern and southern halo orbits at JC = 3.1694

This example demonstrates another advantage of implementing low thrust techniques for transfer design in the cislunar region. The added freedom of the continuous control allows for much shorter time of flight transfers than that of the natural dynamics. This time reduction coincides with a small increase in propellant mass due to the high I_{sp} of the engine. Additionally, the spatial heteroclinic transfers exist as point solutions. They tend to be challenging to compute and are not guaranteed to exist between any two orbits of the same Jacobi Constant without impractically long times of flight. In contrast low thrust transfers can be constructed through intermediate orbit segments for any two orbits of the same family regardless of their energy levels.

6.2 Leveraging Manifolds

Orbits of different families do not have clear intermediate orbits to act as initial guesses for the targeting process. Transfers for these scenarios often involve movement between different regions of cislunar space. Stable and unstable manifolds are employed for these applications. As has been demonstrated in impulsive transfer design, stable and unstable manifolds can be leveraged as initial guesses for transfers between orbits of different families [20].

To form the initial guesses for the optimization process, the unstable manifold of the source orbit and the stable manifold of the sink orbit are propagated around the lunar vicinity for a long period of time. The goal of this process is to find locations where the manifolds nearly intersect in full six dimensional space. If there is a location where the manifolds perfectly intersect then a free, heteroclinic transfer, exists between the orbits and low thrust is not necessary. However, there is no guarantee that these free transfers exist between any two orbits and when they do exists they may have very long times of flight as demonstrated in the previous section.

Manifold arcs that nearly coincide in six dimensional space are corrected for full continuity using low thrust. In order to find these close manifold arcs a hyperplane is constructed. Only manifold states at hyperplane crossings are considered thereby reducing the dimensionality of the problem by one. The hyperplane crossings are viewed on a poincare map to identify near intersections between the stable and unstable arcs. The position of points on the poincare map along with the hyper plane location fully constrains the position of any hyperplane crossing however additional visualization is necessary to determine the velocity of the states. The velocity information is indicated by arrows originating at each point as implemented by Haapala [20]. Thus A good initial guess is computed from hyperplane crossings that nearly coincide on the map and have arrows of similar length and direction.

A transfer between an L1 northern halo and L2 southern halo at a Jacobi Constant of 3.09 is computed to demonstrate the methodology. The orbit information is described in Table 6.8. Manifold arcs of each orbit are propagated for a long period of time depending on the application. For this investigation manifold arcs are propagated for 34 days. Therefore

any initial guess has a maximum TOF of 64 days, but this maximum is not reached in any of the assessed mission scenarios. Selecting too short a propagation time results in very few plane crossings and therefore few opportunities for connections. Too long of a propagation time results in overly long time of flight transfers. However, the propagation time and hyperplane location are often different depending on the exact orbits between which the transfer occurs. The example manifolds and hyperplane constructed at $x = 1 - \mu$ are presented in Figure 6.23.

Table 6.8. Characteristics of L_1 and L_2 halo orbits for transfer

Parameter	Source Orbit	Sink Orbit
Family	L1 Northern Halos	L2 Southern Halos
Jacobi Constant	3.09	3.09
Period (days)	12.1049	14.1597
z-Amplitude (km)	42,580	49,038
Stability Index ($\|\bar{\lambda}\|_\infty$)	432	339
Initial Position (km)	[0.9045,0,-0.0773]	[1.0691,0,0.0710]
Initial Velocity (km/s)	[0,-0.2993]	[0,0.3187,0]

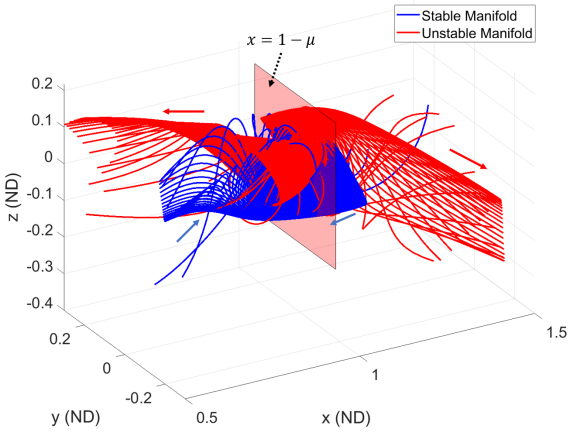

Figure 6.23. Stable manifold of the L_1 northern halo and L_2 southern halo at JC = 3.09 and a hyperplane at $x = 1 - \mu$

In the three dimensional spatial view, identifying possible transit trajectories is extremely challenging. Therefore, the hyperplane is implemented to reduce the dimensionality of the

problem and make selecting the manifold arcs for the initial guess much more straight forward. Figure 6.24 is the hyperplane view of the manifold trajectories. Here, the red represents the unstable manifold crossings of the source orbit and the blue represents the stable manifold crossings of the sink orbit. The position of each point gives the position of the states while the arrows indicate their velocity. The circled points are the closest in full six dimensional space and therefore act as a good initial guess for the transfer. The initial guess computed from the poincare map is depicted in Figure 6.25 The same method is employed

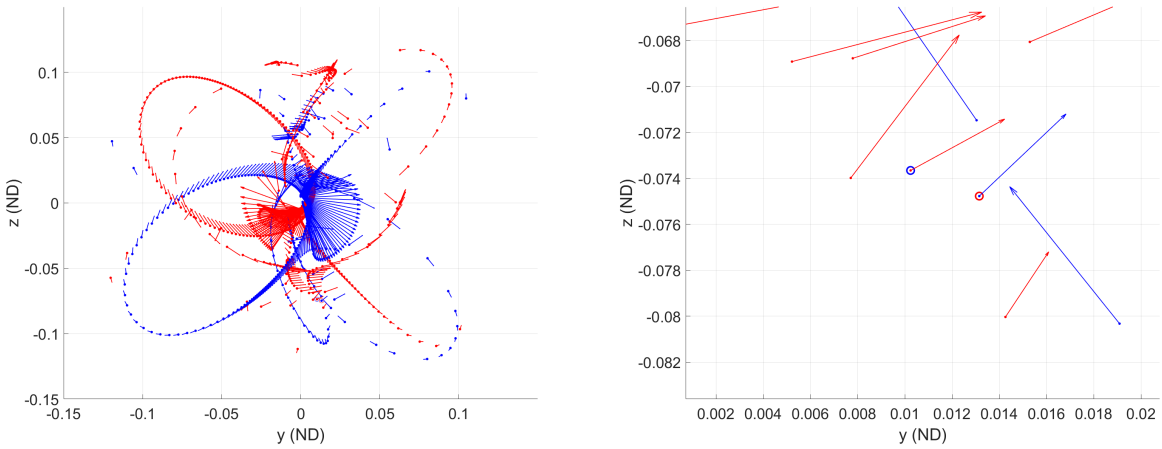

(a) View of all map intersections

(b) Zoomed view on selected manifold arcs

Figure 6.24. Poincare map at $x = 1-\mu$ of L_1 northern halo and L_2 southern halo manifold crossings at JC = 3.09

to convert the initial guess into converged minimum energy, minimum fuel, and IFTT transfers. The optimal transfers and thrust profiles are located in Figure 6.26 while the IFTT and associated thrust profile are in Figures 6.27 and 6.28. Table 6.9 contains the time of flight and propellant mass for each transfer.

Table 6.9. Summary of transfers between L_1 northern and L_2 southren halo orbits

Transfer	Fuel Mass (kg)	Time of Flight (days)
Minimum Energy	3.7491	24.6321
Minimum Fuel	3.2250	24.6321
IFTT	3.3755	24.6598

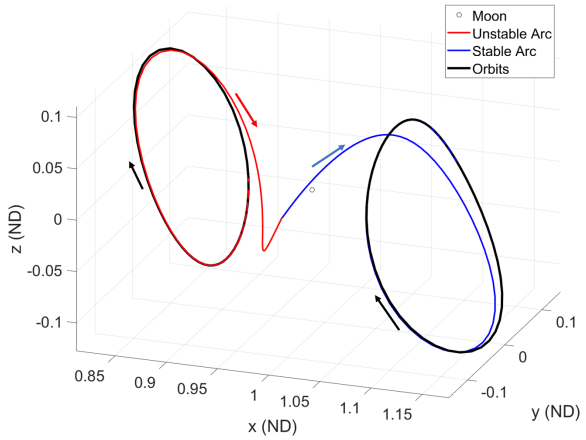

Figure 6.25. Initial guess for the transfer between L_1 northern halo and L_2 southern halo at JC = 3.09

A different mission scenario is considered between the L1 northern halo at a Jacobi Constant of 3.1469 and the L2 southern halo at a Jacobi Constant of 3.1317. The characteristics of the orbits are located in Table 6.10. Because the orbits are of different energy levels, no free transfer exists. The TMDV between the two orbits is computed as 49.2 m/s. However, a lower cost transfer is computed by Haapala [20]. The geometry of this low cost transfer is presented in Figure 6.29. The transfer has a time of flight of 28.9769 days and a single maneuver of 18.2642 m/s. This ΔV cost requires 2.3327 kg of fuel for an impulsive engine as described in Table 6.2. The transfer has a lower ΔV than the theoretical minimum because the maneuver is performed closer to one of the primaries than the orbits.

Table 6.10. Characteristics of L_1 northern and L_2 southern halo orbits with low cost transfer

Parameter	Source Orbit	Sink Orbit
Family	L1 Northern Halos	L2 Southern Halos
Jacobi Constant	3.1496	3.1317
Period (days)	12.0008	14.6532
z-Amplitude (km)	22,560	26,913
Stability Index ($\lvert\bar{\lambda}\rvert_\infty$)	1441	836
Initial Position (km)	[0.8242,0,.0587]	[1.1754,0,-0.0700]
Initial Velocity (km/s)	[0,0.1694,0]	[0,-0.1790,0]

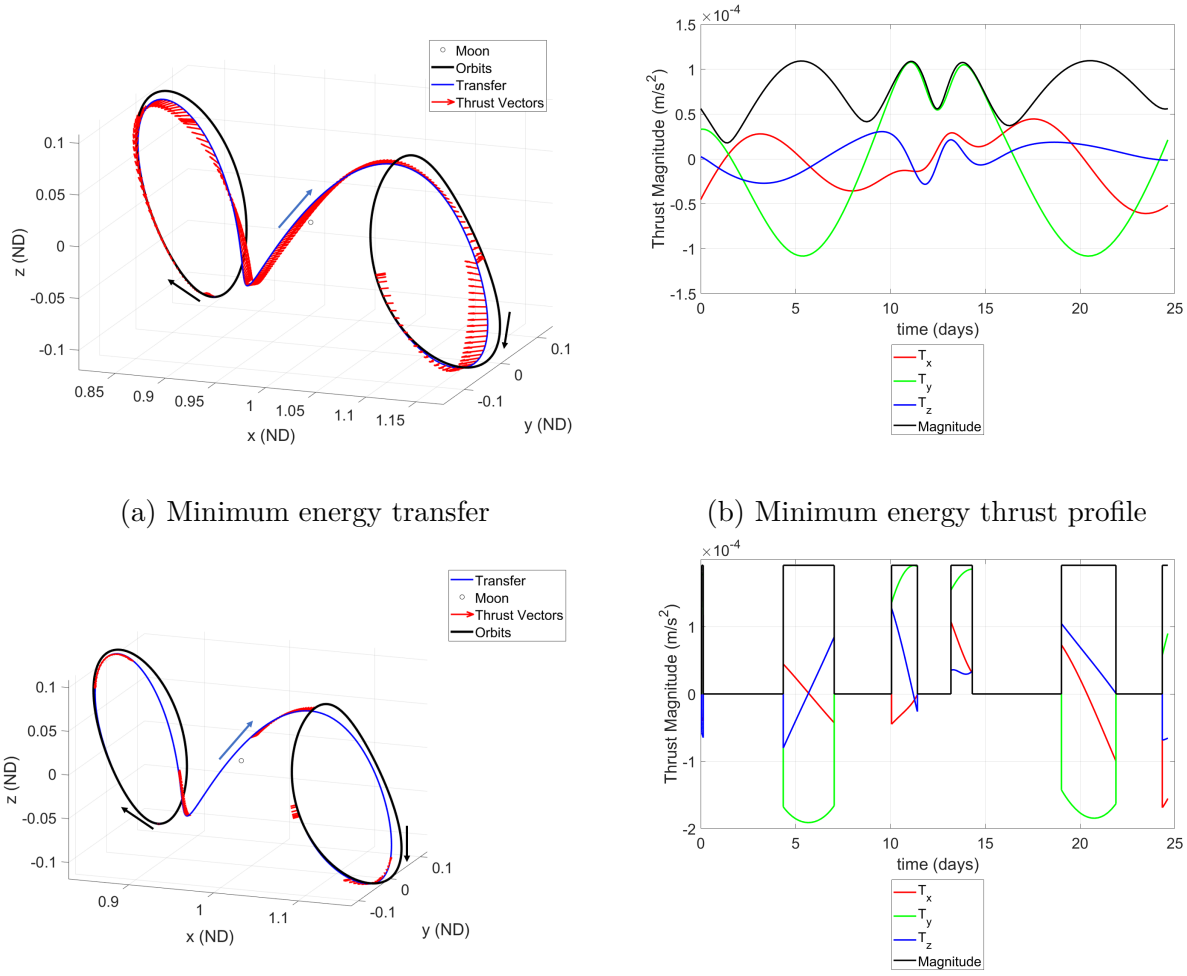

(a) Minimum energy transfer

(b) Minimum energy thrust profile

(c) Minimum Fuel transfer

(d) Minimum fuel thrust profile

Figure 6.26. Optimal transfers and thrust profiles between an L_1 northern halo and L_2 southern halo at JC = 3.09

Targeting is employed to produce optimal low thrust transfers between these orbits. As with the previous example the minimum fuel solution acts as an initial guess for an IFTT. The optimal transfer geometry and thrust profiles are depicted in Figure 6.30, while the final IFTT geometry and thrust profile are depicted in Figures 6.31 and 6.32. A summary of the time of flights and propellant mass consumption of all the transfers are given in Table 6.11. Notice, the IFTT uses less propellant mass and has a shorter time of flight than the impulsive transfer. The low thrust transfers presented in this section leverage the same manifold structures in their construction as their impulsive counterparts. However,

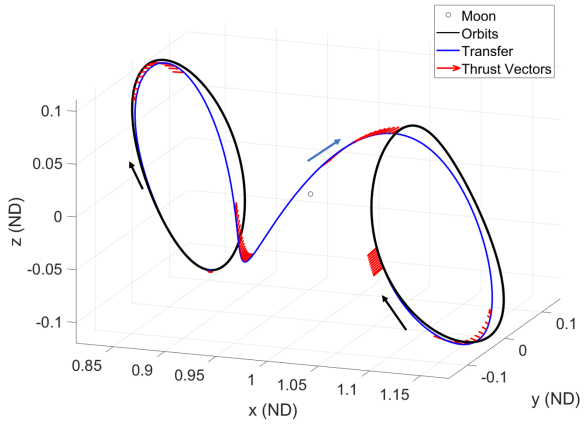

Figure 6.27. IFTT between an L_1 northern halo and L_2 southern halo at JC = 3.09

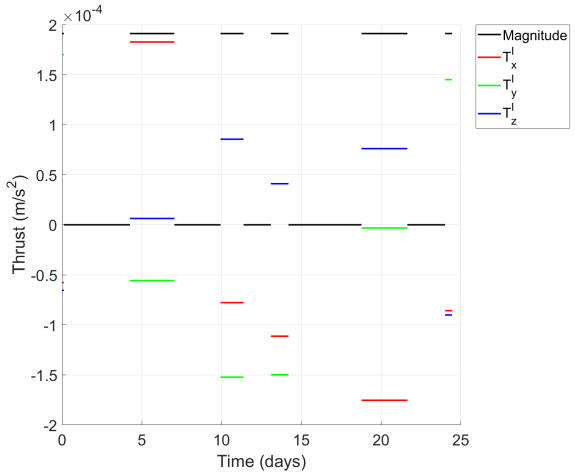

Figure 6.28. IFTT thrust profile between an L_1 northern halo and L_2 southern halo at JC = 3.09

Table 6.11. Summary of transfers between L_1 northern and L_2 southern halo orbits with low cost transfer

Transfer	Fuel Mass (kg)	Time of Flight (days)
Minimum Energy	0.9323	29.8788
Minimum Fuel	0.5346	29.8788
IFTT	0.5737	18.9593
Impulsive Transfer	2.3327	28.9769

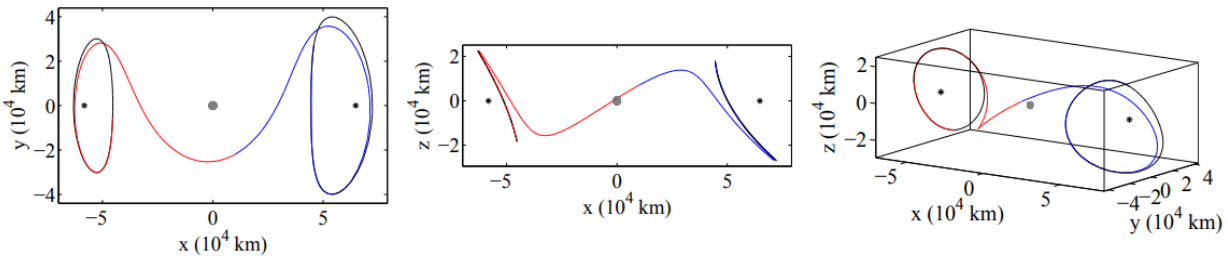

Figure 6.29. Reproduction of Haapala's low cost transfer figure between L_1 northern and L_2 southern halo orbits at JC = 3.1469 and JC = 3.1317

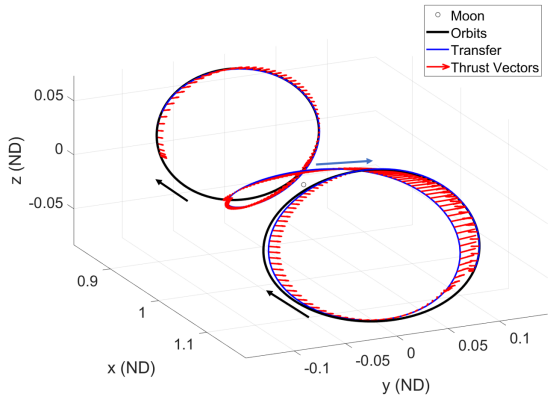

(a) Minimum energy transfer

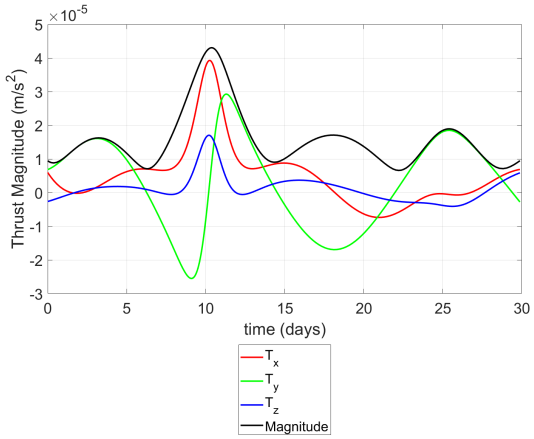

(b) Minimum energy thrust profile

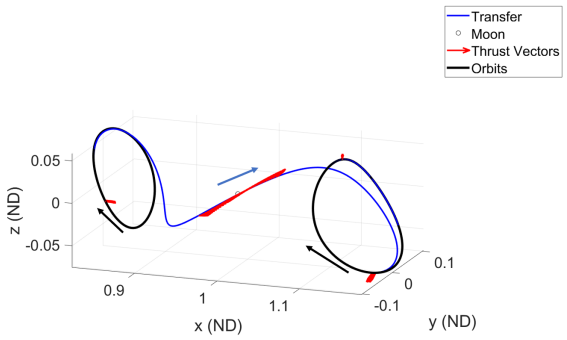

(c) Minimum Fuel transfer

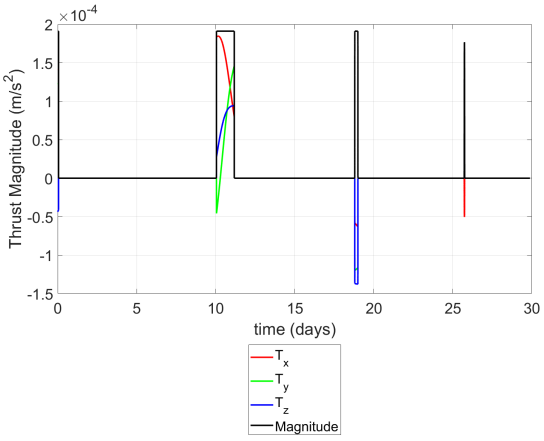

(d) Minimum fuel thrust profile

Figure 6.30. Optimal transfers and thrust profiles between L_1 northern and L_2 southern halo orbits at JC = 3.1469 and JC = 3.1317

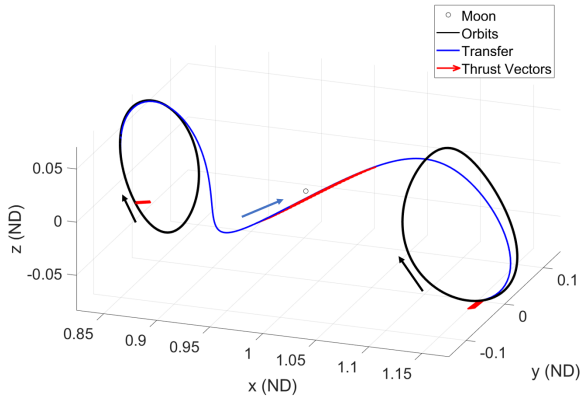

Figure 6.31. IFTT between L_1 northern and L_2 southern halo orbits at JC = 3.1469 and JC = 3.1317

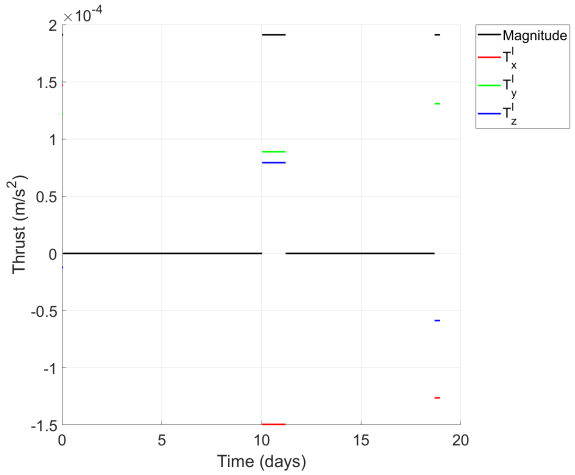

Figure 6.32. IFTT thrust profile between L_1 northern and L_2 southern halo orbits at JC = 3.1469 and JC = 3.1317

the added freedom and efficiency of the low continuous thrust engines produce favorable transfers in many applications. In summary, the low thrust spacecraft model adds flexibility to the mission design process.

6.3 Leveraging Stretching Directions

The previous two sections present effective methods for construction of transfers with particular characteristics. First transfers ar constructed between orbits of the same family. Transfers between different families are constructed through manifolds for unstable orbits. However, a method is necessary for constructing transfers between stable orbits of different families. Selection of intermediate orbits, as an initial guess for these scenarios is challenging and unintuitive. Additionally, the stable nature of the orbits means that no manifolds exist that asymptotically approach and depart the orbits. Instead, stretching directions are employed to inform the direction of impulsive maneuvers. Performing maneuvers along the orbit and propagating in forward and backward time creates manifold-like structures around the orbit. These structures are a form of pseudo-manifold that are useful for cislunar transfer design.

The pseudo-manifold is constructed by computing the most stretching direction for a particular time horizon at several fixed points along the orbit. The stretching direction of the sink orbit is computed in negative time to produce trajectories that quickly approach the orbit from throughout the system. The stretching direction of the source orbit is computed in positive time to construct arcs that quickly depart the orbit. For this investigation the direction corresponding to the greatest final change in state due to the change in initial velocity is computed as described in Chapter 3. A ΔV is applied at each location along the orbit in this most stretching direction. The maneuver magnitude must be large enough to ensure the trajectories escape the stable linear dynamics around the orbit. However, overly large ΔV are harder to remove during the optimal targeting process. The maneuver size is informed by the TMDV between the orbits. If this size of maneuver results in trajectories staying near the orbits from which they originate the magnitude is increased. If the maneuver is too large it is reduced until it produces quick departures as cheaply as possible. The computed stretching direction trajectories are implemented analogously to the manifold trajectories as discussed in the previous section. They are propagated to a hyperplane of interest between the orbits with all crossings of the hyperplane examined for near continu-

ity. An initial guess is produced by examining the hyperplane for near full state continuity between the trajectories.

Unlike the manifold arcs, the stretching direction trajectories do not represent free arrival and departure. The initial guess for the transfer has discontinuities in velocity between the transfer arcs and the source and sink orbits. The manifold arcs initial guess are produced via a small step off from the orbits in full six dimensional space. Th unstable underlying dynamics cause the state to exponentially depart the orbit. However, stable orbits generally need a large manuever to have a similar effect. As a result, the ΔV must be stepped down through a continuation process. A minimum energy transfer is computed between the post maneuver states. This solution is then used as an initial guess for a transfer between states after a slightly smaller maneuver. The process is continued until the impulsive manuevers are completely removed. Once the transfer begins and ends directly on the orbits of interest the locations on the orbits are selected optimally via the transversality condition. After construction of the minimum energy transfer the process is the same as with th previous applications. Minimum fuel and IFTT transfers are constructed leveraging previous transfers as initial guesses.

An example transfer is constructed between a DRO at a JC of 2.9604 and a L4SP at a JC of 2.9132, with a TMDV of 59.1 m/s. These orbits are selected for comparison to the impulsive transfers constructed by Capdevila [49]. The orbit characteristics are located in Table 6.12. Capdevila constructs multiple families of transfers between these two orbits, but for brevity the low thrust transfer is compared to her lowest ΔV transfer as well as a transfer at a local minimum in ΔV with the lowest time of flight. The geometry of these transfers is reproduced in Figure 6.33.

In order to construct the initial guess for this problem, a stretching direction pseudo-manifold is constructed for each orbit. The stretching directions are computed for the STM of a half period to ensure a quick departure. The source orbit uses an STM computed in forward time while the STM of the sink orbit is computed in backward time. A 50 m/s maneuver is applied in the most stretching direction at each point on the orbit and the resulting states are propagated to a hyperplane. The hyperplane is a line on the x-y plane 45 degrees from the x axis intersecting the system barycenter. The two trajectories that

Table 6.12. Characteristics of DRO and L4SPO for transfer

Parameter	Source Orbit	Sink Orbit
Family	DRO	L4SP
Jacobi Constant	2.9604	2.9132
Period (days)	10.0233	28.3508
Stability Index ($\|\bar{\lambda}\|_\infty$)	1	1
Initial Position (km)	[0.8495,0,0]	[0.8232,0.8660,0]
Initial Velocity (km/s)	[0,0.4794,0]	[0.1630,-0.3968,0]

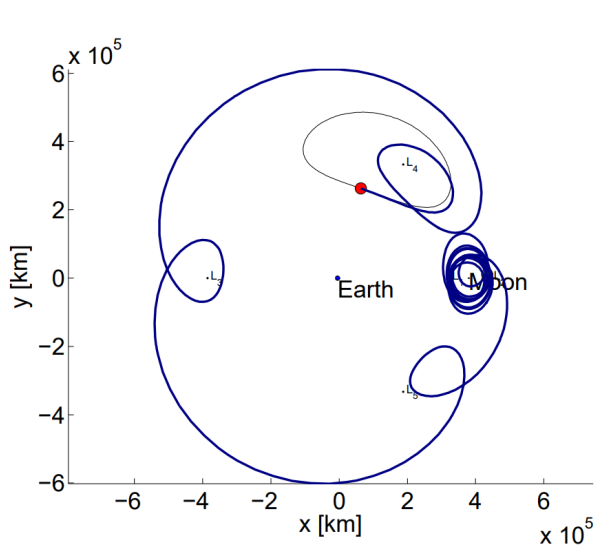

(a) Lowest ΔV transfer

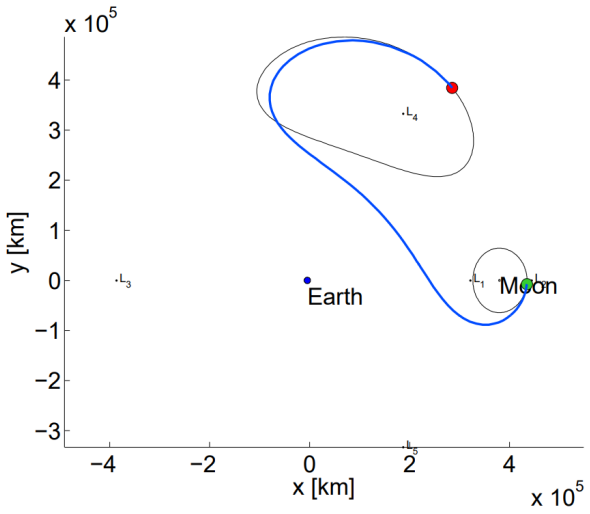

(b) Lowest time of flight local cost minimum transfer

Figure 6.33. Reproduction of Capdevila's transfers between a DRO at JC = 2.9604 and a L4SP at JC = 2.9132

coincide closest at the hyperplane are shown in Figure 6.34. The trajectories act as an initial guess for the transfer design process. The minimum energy transfer, minimum fuel transfer, and IFTT are then produced from this initial guess. The transfers and thrust profiles resulting from the optimization process are depicted in Figure 6.35, while the IFTT geometry and thrust profile are presented in Figures 6.36 and 6.37. The transfers propellant mass requirements and time of flights are listed for comparison in Table 6.13

The value of leveraging the added efficiency of low thrust engines becomes apparent in the stable orbit transfer problem. Due to the stability of the orbits of interest, relatively high ΔV maneuvers are required to quickly depart the orbit vicinity. The time of flight

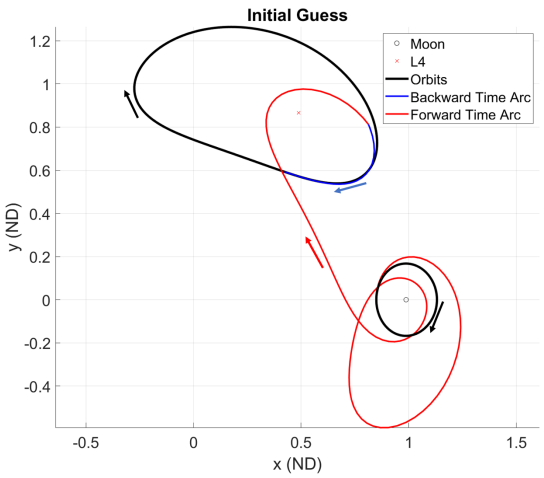

Figure 6.34. Stretching direction initial guess for transfer between DRO and L4SP

Table 6.13. Summary of transfers between DRO and L4SPO

Transfer	Fuel Mass (kg)	Time of Flight (days)
Minimum Energy	3.9229	45.5169
Minimum Fuel	2.8696	45.5169
IFTT	2.9547	44.7154
Min Propellant Impulsive	5.3804	247.439
Short TOF Impulsive	28.1128	21.5816

for the cheaper transfer is much longer because the spacecraft performs several rotations around the moon before finally departing towards L_4. This slow departure is visible in Figure 6.33(a) and cannot be avoided without much larger propellant cost for an impulsive engine. Contrarily, the low thrust transfer is able to depart and arrive on the stable orbits with greater efficiency. It has notable savings in both propellant cost and time of flight. The fast impulsive transfer has a lower TOF than the low thrust transfer but the higher propellant cost may not be practical for all missions.

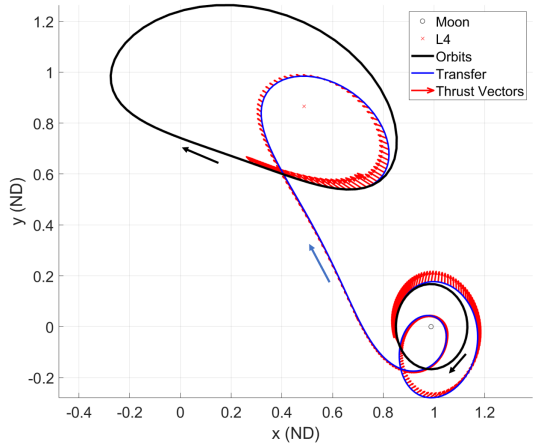

(a) Minimum energy transfer

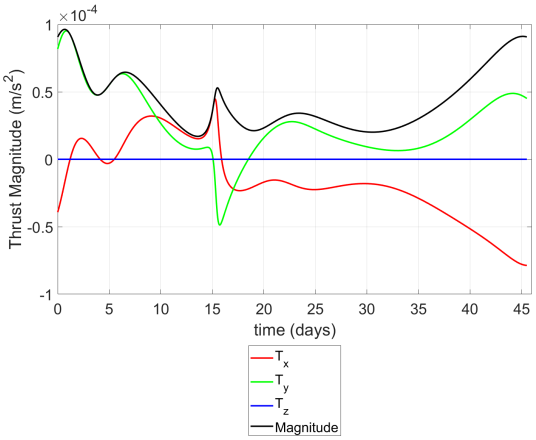

(b) Minimum energy thrust profile

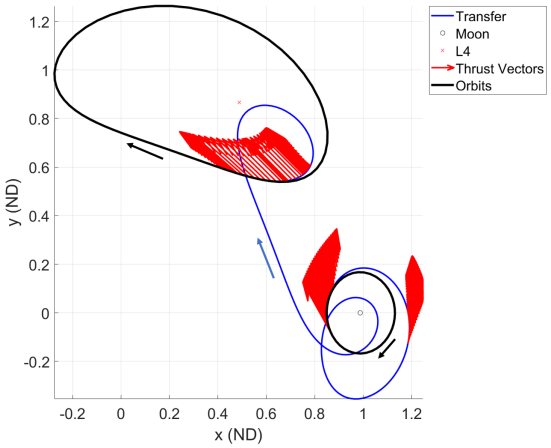

(c) Minimum Fuel transfer

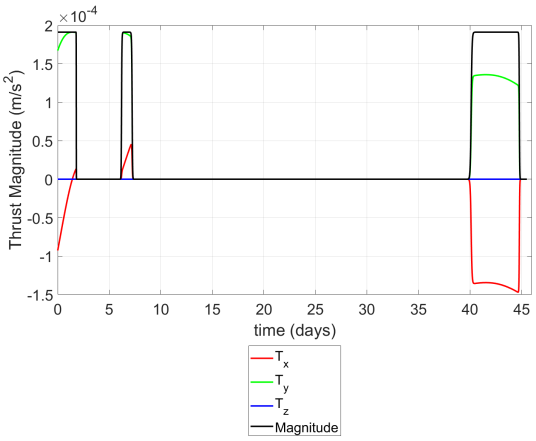

(d) Minimum fuel thrust profile

Figure 6.35. Optimal transfers and thrust profiles between a DRO at JC = 2.9604 and a L4SP at JC = 2.9132

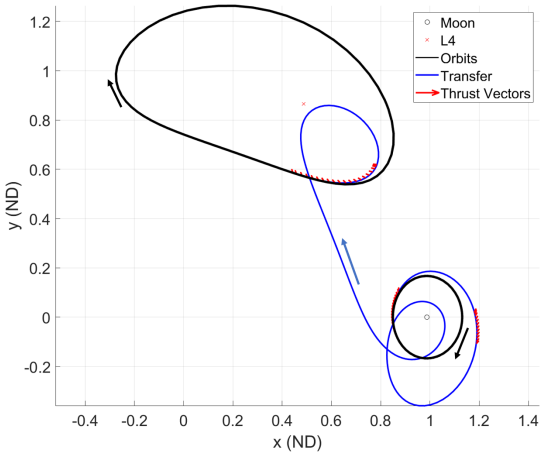

Figure 6.36. IFTT between a DRO at JC = 2.9604 and a L4SP at JC = 2.9132

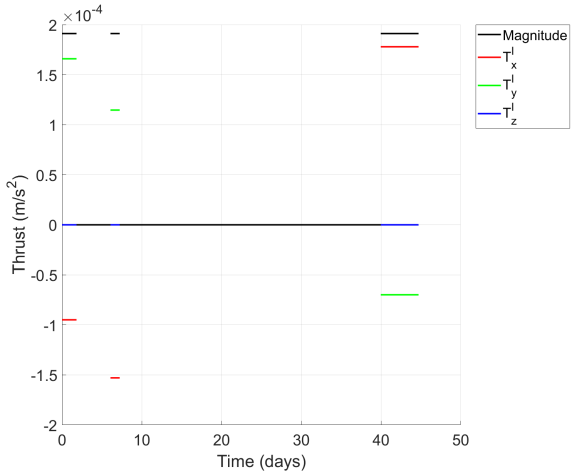

Figure 6.37. IFTT thrust profile between a DRO at JC = 2.9604 and a L4SP at JC = 2.9132

7. CONCLUSION

7.1 Summary

The ability to efficiently traverse cislunar space is of the utmost importance for the expansion of human presence on the Moon. This investigation developes techniques for low thrust transfer design between libration point orbits within the CR3BP. Indirect optimization is employed to compute these transfer with very low propellant cost. The chaotic nature of the CR3BP along with the continuous thrust profile of low thrust transfers create challenges in conventional trajectory design techniques, however leveraging dynamic structures within the mathematical model notably mitigates these challenges. The computed transfers require a fraction of the propellant necessary for impulsive transfers and often have a lower time of flight. In applications where heteroclinic connections exist, low thrust transfers also have lower times of flight than the free heteroclinic transfers for a small propellant cost.

The most prominent challenge when formulating an indirect optimization problem is the initial guess for the costate vector. In general costates do not have any physical interpretation, however setting all costates to zero results in a fully ballistic trajectory. This insight allows dynamic structures to act as an initial guess for the transfer design problem. The resulting initial guesses meet all necessary conditions but not the transversality or continuity constraints. Differential corrections methods are employed to compute an optimal transfer from the initial guess that meets these constraints. Orbits, stable/unstable manifolds, and stretching direction maneuvers are all implemented as ballistic initial guesses. Intermediate orbits define the structure of transfers between orbits of the same family. Stable and Unstable manifolds act as initial guesses between unstable orbits of different families for their ability to traverse cislunar space. Lastly, stretching direction maneuvers are employed to form trajectories that quickly depart and arrive at stable orbits. The maneuvers are stepped down through a continuation process to produce low thrust transfers without an impulsive ΔV.

For ease of convergence, initially a minimum energy solution is produced. These solutions have relatively low propellant requirements and smooth continuous thrust profiles. The minimum energy transfer acts as an initial guess for the minimum fuel solution via sigmoid

smoothing. The resulting transfer requires less propellant mass and has a nearly discrete thrust profile that approximates the optimal bang-coast-bang solution. The final step is to target operational constraints for an Inertially Fixed Thrust Transfer (IFTT). As the name implies the IFTT solution is defined as having thrust acceleration vectors fixed in the inertial frame.

Several transfers are computed in this document to demonstrate th effectiveness of the design process. Multiple transfers are computed between L_1 halo orbits. The resulting transfers have lower propellant requirements than that needed for an impulsive engine to implement a theoretical minimum ΔV maneuver. Transfers are also computed between L_1 and L_2 halo orbits. These require less propellant than low cost impulsive transfers between the same orbits and have lower times of flight than heteroclinic connections. Lastly, a transfer is computed between a stable DRO and L4SPO. The transfer has notable propellant savings compared to the fastest impulsive transfer between the orbits and a much lower time of flight than the minimum ΔV impulsive transfer.

7.2 Future Work

Low thrust transfer construction has many additional avenues of study that can be pursued in future works. Some additional research areas includes:

- Considering additional path constraints for transfers. In general indirect optimization tends to struggle with path constraints. The sigmoid smoothing cleverly circumvents this problem for the constraint of maximum thrust, but other mathematical tools are needed for supplemental constraints such as eclipse avoidance.

- Phasing constraints could also be examined for allowing rendezvous between a spacecraft in the source orbit with a spacecraft in the sink orbit. This added constraint on the phasing would alter the transversality condition and likely increase the fuel required.

- Though the feasibility targeter results in extremely propellant efficient transfers, optimality constraints can be added to this final targeting step. The thrust direction

and duration for each thrust arc are optimized as variables. Therefore the problem is one of function optimization rather than functional optimization. As a result lagrange multipliers are sufficient for the problem as opposed to indirect optimization of costates.

- The plan for NASA Gateway is to become a hub for cislunar spacecraft in the next decade. As a result, transfers to and from the 9:2 near rectilinear halo orbit are an important topic for future research. The low stability index of this orbit implies stretching direction initial guesses are likely more effective than leveraging stable and unstable manifolds.

- All the applications discussed in this investigation involve transfers from one orbit to another. However, further research could be performed to determine optimal transfers between systems of multiple orbits, such as a service satellite moving to multiple customer orbits before returning to a servicing depot.

- All transfers in this investigation are designed in the CR3BP to act as a preliminary design for higher fidelity models. Further investigation is necessary in the transition process of the transfers into an ephemeris model.

REFERENCES

[1] M. Smith *et al.*, "The Artemis Program: An Overview of NASA's Activities to Return Humans to the Moon," in *2020 IEEE Aerospace Conference*, ISSN: 1095-323X, Mar. 2020, pp. 1–10. DOI: 10.1109/AERO47225.2020.9172323.

[2] T. Gardner *et al.*, "CAPSTONE: A CubeSat Pathfinder for the Lunar Gateway Ecosystem," *Small Satellite Conference*, Aug. 2021.

[3] D. Connell and B. R. Zamora, *Gateway: Forward Progress on Artemis IV - NASA*, eng, Section: Artemis, Apr. 2024. Accessed: Aug. 22, 2024. [Online]. Available: https://www.nasa.gov/image-article/gateway-forward-progress-on-artemis-iv/.

[4] M. W. McElwain *et al.*, "The James Webb Space Telescope mission status," eng, ISSN: 0277-786X, vol. 12180, SPIE, 2022, 121800P–121800P–13, ISBN: 1-5106-5341-4.

[5] Q. Moon and D. K. Geller, "Batch Dilution of Precision Optimal Navigation Planning for Cislunar Environments," eng, *The Journal of the astronautical sciences*, vol. 70, no. 6, 2023, Place: New York Publisher: Springer US, ISSN: 2195-0571.

[6] S. Mathavaraj and K. Negi, "Chandrayaan-3 Trajectory Design: Injection to Successful Landing," eng, *Journal of spacecraft and rockets*, pp. 1–8, 2024, ISSN: 0022-4650.

[7] Y. Narusawa, K. Fukuzawa, M. Miyanaga, and N. Tanaka, "Development of 100 kg class small satellite, green propellant reaction control system (gprcs) and thruster/tank for moon lander (slim),mitsubishi heavy industries technical review vol.58 no.4(2021)," *Mitsubishi Heavy Industries Technical Review*, vol. 58, no. 4, 2021.

[8] M. D. Rayman, T. C. Fraschetti, C. A. Raymond, and C. T. Russell, "Dawn: A mission in development for exploration of main belt asteroids Vesta and Ceres," eng, *Acta astronautica*, vol. 58, no. 11, pp. 605–616, 2006, Publisher: Elsevier Ltd, ISSN: 0094-5765.

[9] M. D. Rayman, P. Varghese, D. H. Lehman, and L. L. Livesay, "Results from the Deep Space 1 technology validation mission," eng, *Acta astronautica*, vol. 47, no. 2, pp. 475–487, 2000, Publisher: Elsevier Ltd, ISSN: 0094-5765.

[10] K. C. Howell, "Three-dimensional, periodic, 'halo' orbits," *Celestial Mechanics*, vol. 32, no. 1, pp. 53–71, 1984. DOI: 10.1007/BF01358403.

[11] I. Newton, *The Principia: Mathematical Principles of Natural Philosophy*, trans. by I. Cohen, A. Whitman, and J. Budenz. University of California Press, 1999.

[12] V. G. Szebehely and H. Mark, *Adventures in Celestial Mechanics*, eng, 2nd ed. New York: John Wiley, 1998.

[13] D. H. Gottlieb, "Poincaré and the Three Body Problem. By June Barrow-Green," eng, *The American mathematical monthly*, vol. 106, no. 10, pp. 977–980, 1999, ISSN: 0002-9890.

[14] G. W. Hill, "Researches in the Lunar Theory," eng, *American journal of mathematics*, vol. 1, no. 3, pp. 245–260, 1878, Publisher: American Journal of Mathematics, ISSN: 0002-9327.

[15] 1.-1. Poincaré Henri, *Les méthodes nouvelles de la mécanique céleste / par H. Poincaré .. : v.2*, fre. France: Gauthier-Villars, 1892-1899, 1899, vol. 2.

[16] J. BREAKWELL and J. BROWN, "The 'halo' family of 3-dimensional periodic orbits in the restricted3-body problem," eng, in *Astrodynamics Conference*, 1979.

[17] M. Henon, *Generating families in the restricted three-body problem* (Lecture Notes in Physics Monographs, 52), eng, 1st ed. 1997. Berlin ; Springer, 1997, Publication Title: Generating families in the restricted three-body problem, ISBN: 3-540-69650-4.

[18] W. S. Koon, M. W. Lo, J. E. Marsden, and S. D. Ross, "Heteroclinic connections between periodic orbits and resonance transitions in celestial mechanics," eng, *Chaos: an interdisciplinary journal of nonlinear science*, vol. 10, no. 2, pp. 427–469, 2000.

[19] T. S. Parker and L. O. Chua, *Practical Numerical Algorithms for Chaotic Systems*, eng. New York, NY: Springer New York, 1989.

[20] A. F. Haapala, "Trajectory design in the spatial circular restricted three-body problem exploiting higher-dimensional Poincare maps.," eng, Ph.D. dissertation, Purdue University, 2014, ISBN: 9781321643008.

[21] D. F. LAWDEN, "Rocket trajectory optimization - 1950-1963," eng, *Journal of Guidance, Control, and Dynamics*, vol. 14, no. 4, pp. 705–711, 1991, ISSN: 0731-5090. DOI: 10.2514/3.20703.

[22] B. A. Conway, Ed., *Spacecraft Trajectory Optimization* (Cambridge Aerospace Series). Cambridge: Cambridge University Press, 2010, ISBN: 978-0-521-51850-5. DOI: 10.1017/CBO9780511778025.

[23] J. Stuart, M. Ozimek, and K. Howell, "Optimal, Low-Thrust, Path-Constrained Transfers Between Libration Point Orbits Using Invariant Manifolds," in *AIAA/AAS Astrodynamics Specialist Conference*, ser. Guidance, Navigation, and Control and Co-located Conferences, American Institute of Aeronautics and Astronautics, 2010.

[24] J. Senent, C. Ocampo, and A. Capella, "Low-Thrust Variable-Specific-Impulse Transfers and Guidance to Unstable Periodic Orbits," eng, *Journal of guidance, control, and dynamics*, vol. 28, no. 2, pp. 280–290, 2005, ISSN: 0731-5090. DOI: 10.2514/1.6398.

[25] N. L. O. Parrish, "Low Thrust Trajectory Optimization in Cislunar and Translunar Space," eng, ISBN: 9780438382602, Ph.D. dissertation, University of Colorado at Boulder, 2018.

[26] J. M. Longuski, J. J. Guzmán, and J. E. Prussing, *Optimal Control with Aerospace Applications* (Space Technology Library ; 32), eng, 1st ed. 2014. New York, NY: Springer New York, 2014, ISBN: 1-4614-8945-8. DOI: 10.1007/978-1-4614-8945-0.

[27] A. D. Cox, "A Dynamical Systems Perspective for Preliminary Low-Thrust Trajectory Design in Multi-Body Regimes," eng, Ph.D. dissertation, Purdue University, 2020.

[28] B. J. P. Pino, "Energy-Informed Strategies for Low-Thrust Trajectory Design in Cislunar Space," eng, Ph.D. dissertation, Purdue University, 2020.

[29] A. E. Roy and M. W. Ovenden, "On the Occurrence of Commensurable Mean Motions in the Solar System: The Mirror Theorem," *Monthly Notices of the Royal Astronomical Society*, vol. 115, no. 3, pp. 296–309, 1955.

[30] M. Meyer, L. Johnson, B. Palaszewski, D. Coote, D. Goebel, and H. White, *Roadmap for In-Space Propulsion Technology*, eng. Hampton: NASA/Langley Research Center, 2012, Publication Title: NASA Center for AeroSpace Information (CASI). Reports.

[31] N. R. Council, D. o. Engineering, P. Sciences, Aeronautics, S. E. Board, and S. C. f. N. T. Roadmaps, *NASA Space Technology Roadmaps and Priorities: Restoring NASA's Technological Edge and Paving the Way for a New Era in Space*, eng, 1st ed. Headquarters: National Academies Press, 2012, Backup Publisher: Steering Committee for NASA Technology Roadmaps, ISBN: 978-0-309-25362-8.

[32] Z. You, *Space Microsystems and Micro/Nano Satellites*, eng. United States: Elsevier Science & Technology, 2017, pp. 295–339, ISBN: 0-12-812672-8.

[33] M. L. McGuire, S. L. McCarty, K. Hack, and S. N. Karn, "Application of Solar Electric Propulsion to the Low Thrust Lunar Transit of the Gateway Power and Propulsion Element," eng, *the International Electric Propulsion Conference*, 2024.

[34] T. H. Gronwall, "Note on the Derivatives with Respect to a Parameter of the Solutions of a System of Differential Equations," eng, *Annals of mathematics*, vol. 20, no. 4, pp. 292–296, 1919.

[35] D. J. Grebow, "Trajectory design in the Earth-Moon system and lunar South Pole coverage.," eng, Ph.D. dissertation, Purdue University., 2010.

[36] W. E. Wiesel and D. J. Pohlen, "Canonical Floquet theory," eng, *Celestial Mechanics and Dynamical Astronomy*, vol. 58, no. 1, pp. 81–96, 1994.

[37] L. Perko, *Differential Equations and Dynamical Systems* (Texts in Applied Mathematics), J. E. Marsden, L. Sirovich, and M. Golubitsky, Eds. New York, NY: Springer, 2001, vol. 7. DOI: 10.1007/978-1-4613-0003-8.

[38] V. Muralidharan, "Stretching Directions in Cislunar Space: Stationkeeping and an Application to Transfer Trajectory Design," eng, Ph.D. dissertation, Purdue University, 2021.

[39] G. Haller, "A variational theory of hyperbolic Lagrangian Coherent Structures," *Physica D: Nonlinear Phenomena*, vol. 240, no. 7, pp. 574–598, 2011.

[40] L. S. (S. Pontriagin, *The mathematical theory of optimal processes* ([International series of monographs on pure and applied mathematics, v. 55]), eng. New York: Interscience Publishers, 1962.

[41] O. Bolza, *Lectures on the calculus of variations; by Oskar Bolza*, eng. Illinois: The University of Chicago press, 1904.

[42] A. E. Bryson and Y.-C. Ho, *Applied optimal control: optimization, estimation, and control*, eng. New York, New York ; Taylor and Francis, 1975, ISBN: 978-1-351-46591-5.

[43] T. Haberkorn, P. Martinon, and J. Gergaud, "Low thrust minimum-fuel orbital transfer: A homotopic approach," eng, *Journal of Guidance Control and Dynamics*, vol. 27, no. 6, pp. 1046–1060, Nov. 2004, ISSN: 0731-5090. DOI: 10.2514/1.4022.

[44] R. Bertrand and R. Epenoy, "New smoothing techniques for solving bang-bang optimal control problems - numerical results and statistical interpretation," eng, *Optimal Control Applications and Methods*, vol. 23, no. 4, pp. 171–197, Jul. 2002, ISSN: 1099-1514. DOI: 10.1002/oca.709.

[45] E. Taheri, I. Kolmanovsky, and E. Atkins, "Enhanced Smoothing Technique for Indirect Optimization of Minimum-Fuel Low-Thrust Trajectories," eng, *Journal of guidance, control, and dynamics*, vol. 39, no. 11, pp. 2500–2511, 2016, ISSN: 0731-5090. DOI: 10.2514/1.G000379.

[46] E. Taheri and J. L. Junkins, "Generic Smoothing for Optimal Bang-Off-Bang Spacecraft Maneuvers," eng, *Journal of guidance, control, and dynamics*, vol. 41, no. 11, pp. 2470–2475, 2018, ISSN: 0731-5090. DOI: 10.2514/1.G003604.

[47] N. B. LaFarge, "Reinforcement Learning Approaches for Autonomous Guidance and Control in a Low-Thrust, Multi-body Dynamical Environment," eng, Ph.D. dissertation, Purdue University, United States – Indiana, 2023.

[48] J. R. Stuart, "Fuel-optimal, low-thrust transfers between libration point orbits.," eng, M.S. thesis, Purdue University., 2011.

[49] L. R. Capdevila, "A transfer network linking Eearth, Moon, and the triangular libration point regions in the Earth-Moon system," eng, Ph.D. dissertation, Purdue University, 2016.